CELL BIOLOGY

Inter-organelle cross-talk supports acetyl-coenzyme A homeostasis and lipogenesis under metabolic stress

Ramya S. Kuna[1,2]†, Avi Kumar[1,2]†, Karl A. Wessendorf-Rodriguez[1,2], Hector Galvez[1], Courtney R. Green[1,2], Grace H. McGregor[1,2], Thekla Cordes[1,2,3], Reuben J. Shaw[1], Robert U. Svensson[4], Christian M. Metallo[1,2]*

Proliferating cells rely on acetyl-CoA to support membrane biogenesis and acetylation. Several organelle-specific pathways are available for provision of acetyl-CoA as nutrient availability fluctuates, so understanding how cells maintain acetyl-CoA homeostasis under such stresses is critically important. To this end, we applied ^{13}C isotope tracing cell lines deficient in these mitochondrial [ATP-citrate lyase (ACLY)]–, cytosolic [acetyl-CoA synthetase (ACSS2)]–, and peroxisomal [peroxisomal biogenesis factor 5 (PEX5)]–dependent pathways. ACLY knockout in multiple cell lines reduced fatty acid synthesis and increased reliance on extracellular lipids or acetate. Knockout of both ACLY and ACSS2 (DKO) severely stunted but did not entirely block proliferation, suggesting that alternate pathways can support acetyl-CoA homeostasis. Metabolic tracing and PEX5 knockout studies link peroxisomal oxidation of exogenous lipids as a major source of acetyl-CoA for lipogenesis and histone acetylation in cells lacking ACLY, highlighting a role for inter-organelle cross-talk in supporting cell survival in response to nutrient fluctuations.

INTRODUCTION

Acetyl-CoA is a critical precursor for acetylation and lipid synthesis associated with membrane biogenesis, energy storage, and protein modification (*1*). Central carbon metabolism is wired with several redundancies in place to maintain acetyl-CoA homeostasis under conditions of stress, with mitochondria, peroxisomes, and cytosolic acetate activation all contributing to this metabolic pool. While both healthy tissues and tumors readily incorporate lipids from the diet (*1*), de novo lipogenesis (DNL) is required for some tumors and cell types to proliferate (*2*, *3*), how each of these pathways and organelles fuel lipogenesis is not fully clear. Fatty acids are synthesized from two carbon acyl-units provided by cytosolic acetyl-CoA, which is metabolized to malonyl-CoA by acetyl-CoA carboxylase (ACC) and used by fatty acid synthase (FASN) to generate long-chain fatty acids. These fatty acids can be further elongated, desaturated, and incorporated into lipids within the endoplasmic reticulum (ER). In the context of cancer, FASN inhibition reduces body weight (*4*), oncogene expression (*5*), and in vivo growth (*6*) of human breast cancer cell lines in mice. Knockout and pharmacological inhibition of ACC also compromise tumor growth in xenograft and genetically engineered mouse models of lung cancer while synergizing with chemotherapy (*7*).

ATP-citrate lyase (ACLY) is the major conduit through which mitochondrial metabolism supports acetyl-CoA generation, which is important for lipid synthesis as well as epigenetic regulation and DNA repair via histone acetylation (*8*–*10*). Up-regulation of ACLY expression has been identified in a number of numerous cancers up-regulate ACLY expression compared to surrounding healthy tissue, including breast, liver, bladder, stomach, colorectal, glioblastoma, and lung cancers (*11*–*17*), and in patients with gastric adenocarcinoma (*18*) and lung adenocarcinomas (*17*), overexpression and activation of ACLY is associated with poor prognosis. Further, both pharmacological inhibition and genetic knockdown of ACLY have been demonstrated to reduce lipogenesis and cancer cell proliferation (*19*–*26*), supporting the link between ACLY activity and tumor growth. On the other hand, nutrient availability and mitochondrial metabolism are sometimes compromised in cells within the tumor microenvironment, and pathways like reductive carboxylation are often unable to fully compensate (*27*, *28*). Therefore, characterization of alternative acetyl-CoA sources may be useful for understanding cancer cell survival and resistance mechanisms.

The acetyl-CoA synthetase family of enzymes (ACSS1, ACSS2, and ACSS3) are the rate-limiting enzymes involved in acetate activation to acetyl-CoA in mammalian cells (*29*). While ACSS1 and ACSS3 are mitochondrially expressed and tissue-restricted (in the case of ACSS3), ACSS2 is localized in the cytosol (*30*). ACSS2 has garnered interest as a cancer target as high expression of ACSS2 is associated with poor prognosis in breast, glioblastoma, ovarian, and lung cancers (*31*–*33*). Nutrient deprivation, including hypoxia and lipid depletion, up-regulates ACSS2 expression and acetate catabolism for DNL in cancer cells, suggesting that ACSS2 provides a mode of metabolic plasticity to cancer cells under stress (*34*). Hepatocyte-selective depletion of ACSS2 or ACLY decreased liver acetyl-CoA levels in obese mice (*35*). Furthermore, mouse embryonic fibroblasts (MEFs) deficient in ACLY up-regulate ACSS2 protein expression and increase utilization of acetate for cytosolic acetyl-CoA generation (*36*), highlighting the essentiality of acetyl-CoA and metabolic flexibility of proliferative cells.

Peroxisomes generate acetyl-CoA via β-oxidation of fatty acids, most often very long-chain (VLCFA) or branched-chain fatty acids (BCFA), which contribute to malonyl-CoA and lipids in the heart and liver (*37*–*40*). Peroxisomal enzymes involved in oxidation of BCFA (hydroxysteroid 17-beta dehydrogenase 4 and acyl-coenzyme

[1]Department of Molecular and Cell Biology, Salk Institute for Biological Studies, La Jolla, CA 92037, USA. [2]Department of Bioengineering, University of California, San Diego, La Jolla, CA 92093, USA. [3]Department of Bioinformatics and Biochemistry, Braunschweig Integrated Centre of Systems Biology (BRICS), Technische Universität Braunschweig, Braunschweig 38106, Germany. [4]Nimbus Therapeutics, Cambridge, MA 02139, USA.
*Corresponding author. Email: metallo@salk.edu
†These authors contributed equally to this work.

A oxidase 3) are overexpressed in cancerous prostate tissue compared to paired healthy tissue (*41*), suggesting that this organelle may support generation of acetyl-CoA in tumors. However, the extent to which peroxisomal β-oxidation of fatty acids serves as a source of lipogenic acetyl-CoA in cancer cells under nutrient stress warrants further exploration.

Here, we apply mass spectrometry, stable isotope tracing, and isotopomer spectral analysis (ISA) to analyze the metabolic rewiring that occurs when acetyl-CoA synthesis is systematically compromised in cancer cells. We genetically engineered cancer cell lines deficient in ACLY and/or ACSS2 using CRISPR-Cas9. While knockout of ACLY decreased DNL under basal conditions, cells are able to sustain FASN flux and/or growth through use of exogenous acetate or serum lipids. On the other hand, knockout of both ACLY and ACSS2 induces a growth-limiting stress regardless of medium nutrient status. Last, we observe that ACLY-deficient cells use peroxisomal β-oxidation as a substantial source of lipogenic acetyl-CoA and are sensitive to peroxisomal biogenesis factor 5 (PEX5) knockout or pharmacological inhibition of peroxisomal β-oxidation. Collectively, our study highlights the rewiring of organelle-specific acetyl-CoA metabolism in fueling DNL when mitochondrial (ACLY), cytosolic (ACSS2), and peroxisomal (PEX5) CoA sources are compromised in cancer cells.

RESULTS

ACLY deficiency compromises fatty acid synthesis and drives lipid dependence of cell lines

To understand how ACLY and ACSS2 contribute to fatty acid synthesis (Fig. 1A), we generated *ACLY*-knockout (*ACLY*-KO) clones using CRISPR-Cas9 in A549 human non–small cell lung cancer (NSCLC) cells, 634T murine NSCLC cells, HepG2 hepatocarcinoma cells, and HAP1 cells (Fig. 1B and fig. S1A). We observed increased protein expression of ACSS2 in the A549 and HepG2 *ACLY*-KO cell lines (Fig. 1B and fig. S1A), consistent with previous results in MEFs (*36*). The growth rate of the *ACLY*-KO A549, 634T, and HAP1 cells was marginally lower compared to wild-type (WT) cells, while HepG2 *ACLY*-KO cells showed an over 50% reduction in growth rate compared to the WT cells (Fig. 1C and fig. S1B). In A549 cells, *ACLY*-KO resulted in decreased glucose uptake/lactate secretion and increased glutamine uptake/glutamate secretion, suggesting rewiring of central carbon metabolism (Fig. 1D). To better understand how ACLY deficiency alters intracellular metabolism, we cultured A549 clones in the presence of [U-$^{13}C_6$]glucose or [U-$^{13}C_5$]glutamine and quantified isotope enrichment in downstream metabolite pools. Enrichment of tricarboxylic acid (TCA) cycle intermediates from glutamine in A549 *ACLY*-KO cells was elevated, consistent with extracellular flux results (Fig. 1E). These findings may indicate that ACLY-KO induces oxidative stress, as increased glutamine catabolism has been found to be integral to maintaining redox homeostasis in cancer cells through multiple mechanisms (*42*, *43*). On the other hand, glucose enrichment in malate and aspartate (a readout of oxaloacetate) was increased, likely due to decreased generation of acetyl-CoA via ACLY and glutamine-dependent reductive carboxylation (fig. S1C).

HepG2 cells express the plasma membrane citrate transporter solute carrier family 13 member 5 (*44*), so we next used [2,4-$^{13}C_2$]citrate to directly trace the ACLY reaction in HepG2 *ACLY*-KO cells. Catabolism of [2,4-$^{13}C_2$]citrate provides insight into compartment-specific metabolism as M2 labeling of TCA intermediates will result from direct mitochondrial catabolism of labeled citrate, while M1 isotopologs will be formed if the tracer is first catabolized in the cytosol by ACLY (fig. S1D). When culturing HepG2 WT and *ACLY*-KO cells in the presence of 500 μM [2,4-$^{13}C_2$]citrate, we found that the ratio of M1/M2 labeling on malate, aspartate, succinate, and fumarate was significantly decreased in the *ACLY*-KO cells (fig. S1E). Furthermore, the relative abundance of M2 alpha-ketoglutarate was comparable to M1 labeling in WT cells but was significantly greater in the *ACLY*-KO cells (fig. S1F). In addition, enrichment of palmitate was minimal in the *ACLY*-KO cells compared to WT (fig. S1G). These labeling patterns confirm that *ACLY*-KO forces cells to oxidize citrate in the mitochondria and/or cytosol to alpha-ketoglutarate at the expense of acetyl-CoA generation. Next, we applied ISA to quantify palmitate synthesis and the contribution of [U-$^{13}C_6$]glucose to the lipogenic acetyl-CoA pool. ACLY deficiency profoundly decreased palmitate synthesis compared to control cells (Fig. 1F and fig. S1, H and I). Notably, *ACLY*-KO cells maintained some flux from [U-$^{13}C_6$]glucose to lipogenic acetyl-CoA such that ~20% of palmitate carbon was derived from glucose in A549 and HepG2 cells, while a smaller decrease was observed in 634T cells (Fig. 1G and fig. S1J). Collectively, these results indicate that ACLY deficiency effectively decreases FASN flux and alters cytosolic citrate shuttling under normal culture conditions while reducing growth slightly.

Acetate metabolism by ACSS2 supports lipogenesis to enable growth of ACLY-deficient cells

Under conditions where glucose-derived citrate is limiting, such as hypoxia, acetate can be "activated" by acetyl-CoA synthetase enzymes. As protein expression of ACSS2 was markedly increased in *ACLY*-KO cells (Fig. 1B and fig. S1A), we hypothesized that acetate utilization may compensate for loss of ACLY. Supplementation of 1 mM [1,2-$^{13}C_2$] acetate to cultures rescued palmitate synthesis in cells lacking ACLY (Fig. 2A and fig. S2A). Acetate became the primary lipogenic substrate in all tested *ACLY*-KO cell lines (Fig. 2B and fig. S2B) but only contributed between 5 and 40% of lipogenic acetyl-CoA pools in control cells. De novo palmitate synthesis was rescued in the *ACLY*-KO cells grown with acetate (Fig. 2A and fig. S2A) compared to those grown in the absence of acetate (Fig. 1F and fig. S1, F and G) in all cell lines. We also measured the growth rate of control and ACLY-deficient cell lines in various culture media. *ACLY*-KO cells grew comparably to control cells in media supplemented with 10% dialyzed fetal bovine serum (dFBS) (Fig. 2C and fig. S2C); however, when we removed serum, lipid growth of all *ACLY*-KO cells was severely compromised (Fig. 2C and fig. S2C). Addition of 1 mM exogenous acetate enhanced the growth of all *ACLY*-KO cell lines while having no impact on growth rates of control cells (Fig. 2C and fig. S2C). The most marked growth impact of acetate was observed in cultures grown in delipidated serum (Fig. 2C and fig. S2C), highlighting the importance of this metabolic redundancy in supporting acetyl-CoA for lipid synthesis (Fig. 2D).

To confirm the role of ACSS2 in supporting lipogenesis, we examined the growth and metabolism of A549 and HepG2 cells lacking ACSS2 (Fig. 3A and fig. S3A). While ACLY expression was unchanged in *ACSS2*-KO cells (Fig. 3A and fig. S3A), the conversion of [1,2-$^{13}C_2$]acetate to palmitate was significantly decreased (Fig. 3B and fig. S3B), and there was no impact on palmitate

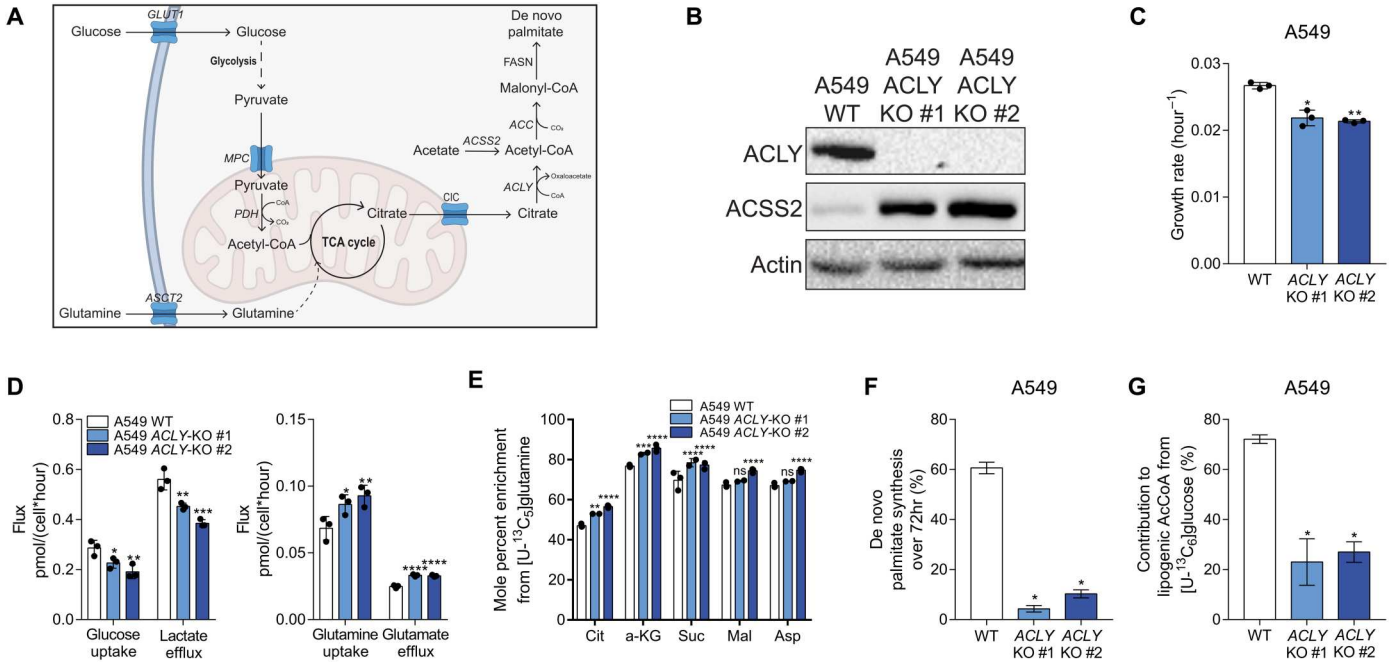

Fig. 1. ACLY-KO rewires central carbon metabolism and leads to a reduction of palmitate synthesis in cancer cells. (**A**) Canonical DNL pathway. (**B**) Western blots of ACLY, ACSS2, and actin in A549 WT and ACLY-KO cells. (**C**) Growth rates of A549 WT and ACLY-KO cells grown in high-glucose Dulbecco's modified Eagle's medium (DMEM) + 10% FBS for 4 days. (**D**) Glucose uptake, lactate efflux (left) and glutamine uptake, glutamate efflux (right) in A549 WT and ACLY-KO cells cultured in high-glucose DMEM + 10% dFBS for 72 hours ($n = 3$). (**E**) Mole percent enrichment of TCA intermediates from [U-13C5]glutamine in A549 ACLY-KO clones cultured in high-glucose DMEM + 10% dFBS for 72 hours ($n = 3$). (**F**) De novo synthesis of palmitate in A549 ACLY-KO cells cultured in high-glucose DMEM + 10% dFBS for 72 hours ($n = 3$). (**G**) Percent of lipogenic acetyl-CoA contributed by [U-13C6]glucose based on ISA modeling in A549 ACLY-KO cells cultured in high-glucose DMEM + 10% dFBS 72 hours ($n = 3$). In (C) to (G), data are plotted as means ± SD. Statistical significance is relative to WT as determined by one-way analysis of variance (ANOVA) with Dunnett's method for multiple comparisons (C) to (E) with $^*P < 0.05$, $^{**}P < 0.01$, $^{***}P < 0.001$, and $^{****}P < 0.0001$. In (F) and (G) *data are plotted as mean estimated flux ± 95% confidence intervals generated via parameter continuation in INCA. Unless indicated, all data represent biological triplicates. Data shown are from one of at least two separate experiments. See also fig. S1. ns, not significant.

synthesis rates in cells lacking ACSS2 (Fig. 3C and fig. S3C). Furthermore, the growth rates of both A549 and HepG2 cell lines were minimally affected by *ACSS2*-KO in lipid-replete medium (Fig. 3D and fig. S3D). However, HepG2 ACSS2-KO cells observed a significant growth defect compared to WT in lipid-depleted media (fig. S3D), matching previous studies which found that ACSS2-KD was detrimental to cancer cell growth in conditions of metabolic stress (*31*, *34*). A549 ACSS2-KO cell growth remained unaffected by media delipidation (Fig. 3D). A similar phenotype bifurcation between the cell lines was observed previously, as HepG2 cells exhibited a greater growth rate reduction upon loss of ACLY compared to A549 cells (Fig. 1C and fig. S1B). mRNA expression of ACSS1 and ACSS3, both mitochondrial isozymes of ACSS2, were significantly elevated in HepG2 hepatocarcinoma cells compared to A549 NSCLC cells (Fig. 3E). Furthermore, [1,2-$^{13}C_2$]acetate enrichment of TCA intermediates was substantially higher in HepG2 cells compared to A549 cells (Fig. 3, F and G), suggesting that mitochondrial ACSS1 and/or ACSS3 compete with cytosolic ACSS2 for utilization of acetate and likely reflecting the metabolism in their tissues of origin. This metabolic redundancy may influence acetate shuttling to mitochondria, lipid pathways (e.g., ER), and nucleus to affect epigenetic regulation which is altered by ACSS1/2 knockdown (*45*) but also suggests this pathway may not be targetable in all tumor or cell types.

Alternative pathways compensate for combined loss of ACLY and ACSS2

Next, we characterized A549 ACLY/ACSS2 double knockout (*ACLY/ACSS2*-DKO) cells to explore how cancer cells respond to extreme restriction of acetyl-CoA sourcing (Fig. 4A). As expected, growth of A549 *ACLY/ACSS2*-DKO cells was significantly impaired relative to WT in all conditions tested, and we observed no rescue effect with acetate supplementation (Fig. 4B). We also detected little to no isotope enrichment in palmitate from [U-$^{13}C_6$]glucose or [1,2-$^{13}C_2$]acetate in *ACLY/ACSS2*-DKO cells (Fig. 4, C and D), confirming that both pathways were defective in these cells. Mammalian cells do not synthesize polyunsaturated fatty acids (PUFAs) de novo and instead rely on exogenous sources. Incorporation of PUFAs into phosphatidylcholine (PC) and triacylglycerols (TAGs) is elevated in *ACLY* and *ACLY/ACSS2* DKO cells, indicating increased contribution of exogenous fatty acids in membrane lipids in *ACLY*-deficient cells (Fig. 4E and fig. S4, A and B). To further confirm this change in lipids in ACLY-deficient cells, we examined their sensitivity to ferroptosis. PUFA-containing lipids readily undergo peroxidation (*46*), and we found that PUFA-enriched *ACLY/ACSS2*-DKO cells were more susceptible to ferroptosis induced by application of the glutathione peroxidase 4 inhibitor, ML210, compared to WT cells (Fig. 4F). Despite these alterations in lipid metabolism, acetylated histone acH3K27 (Fig. 4G) and whole-cell protein acetylation were maintained in lipid-replete

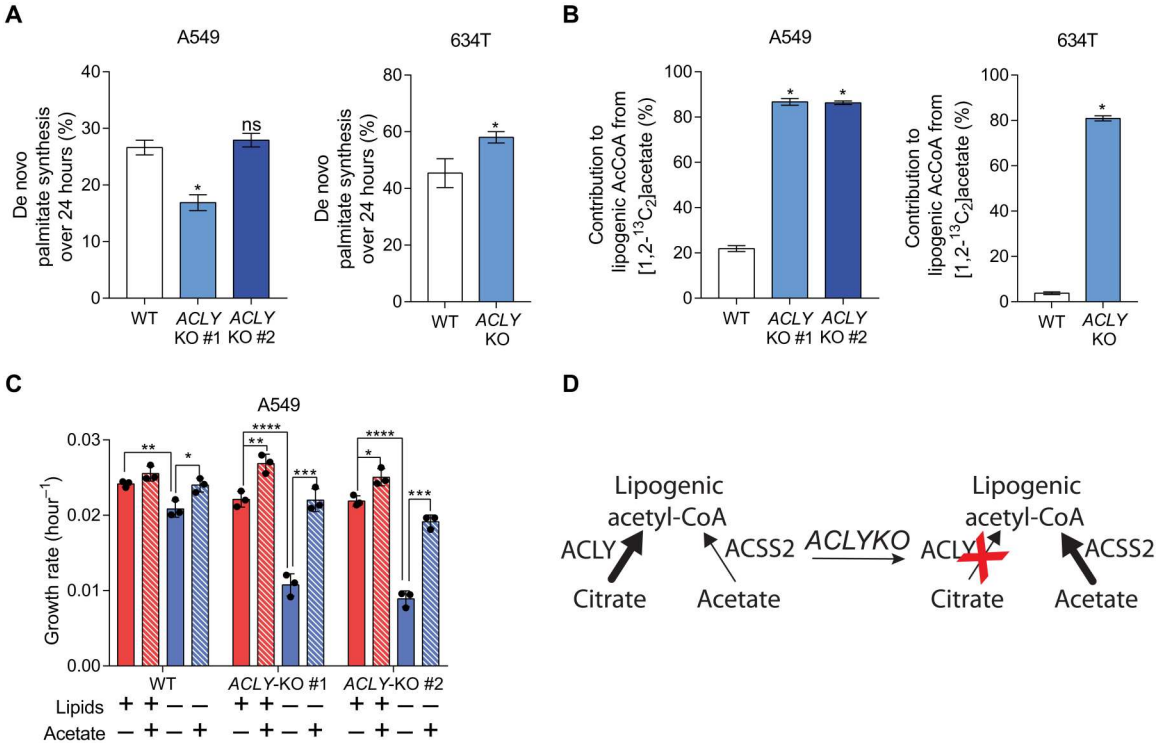

Fig. 2. ACLY-KO growth and fatty acid synthesis are rescued with addition of extracellular acetate. (**A**) De novo synthesis of palmitate in A549 (left) and 634T (right) WT and ACLY-KO cells cultured in high-glucose DMEM + 10% dFBS + 1 mM acetate for 24 hours (n = 3). (**B**) Percent of lipogenic acetyl-CoA contributed by [1,2-13C2]acetate in A549 (left) and 634T (right) and ACLY-KO cells cultured in high-glucose DMEM + 10% dFBS + 1 mM acetate for 24 hours (n = 3). (**C**) Growth rates of A549 WT and ACLY-KO cells grown in high-glucose DMEM + 10% dFBS or delipidated dFBS ± 1 mM acetate for 4 days (n = 3). (**D**) Schematic of lipogenic acetyl-CoA synthesis in ACLY-KO cells. In (A) and (B), *data are plotted as mean estimated flux ± 95% confidence intervals generated via parameter continuation in INCA. In (C), data are plotted as means ± SD. Statistical significance is determined by two-way ANOVA with Tukey's method for multiple comparisons with *P <0.05, **P < 0.01, ***P < 0.001, and ****P < 0.0001. Unless indicated, all data represent biological triplicates. Data shown are from one of at least two separate experiments. See also fig. S2.

ACLY-KO and *ACLY/ACSS2*-DKO cells (fig. S4, C and D), suggesting that NSCLC cells can sustain acetyl-CoA availability through pathways independent of ACLY and ACSS2.

The continued availability of acetyl-CoA for histone acetylation suggests that cancer cells can use alternate pathways for acetyl-CoA generation under conditions of metabolic stress, including non-enzymatic mechanisms (*47*). To explore these pathways more deeply, we cultured A549 *ACLY*-KO and *ACLY/ACSS2*-DKO cells with either ^{13}C-labeled glucose, glutamine, and pyruvate for 72 hours and quantified isotope enrichment in palmitate. In theory, knockout of ACLY will eliminate glucose to palmitate carbon transfer (Fig. 5A); however, A549 *ACLY*-KO cells traced with [U-$^{13}C_6$]glucose continued to sustain labeling on newly synthesized palmitate (Fig. 5B), and we observed similar results with [3-^{13}C]pyruvate (Fig. 5C). Culture of the *ACLY*-KO and *ACLY/ACSS2*-DKO cells with [U-$^{13}C_5$]glutamine yielded insignificant enrichment of palmitate (Fig. 5D), and this pathway was inactive even under hypoxia, where glutamine contributed little to fatty acid synthesis in *ACLY*-KO cells (fig. S5G). These data suggest the existence of a citrate/ACLY-independent lipogenic pathway, which allows glucose and pyruvate but not glutamine to generate acetyl-CoA. We previously demonstrated that carnitine acetyl-transferase (CRAT) actively exports mitochondrial branched-chain-CoAs to enable their elongation to long-chain monomethyl branched-chain fatty acids in adipocytes (*48*), and Izzo *et al.* (*49*) have observed that CRAT facilitates nuclear acetylation and lipogenesis in hepatocellular carcinoma cells. However, we observed minimal labeling of palmitate from [U-$^{13}C_6$]glucose in the A549 *ACLY/ACSS2*-DKO (Fig. 5B), despite noting significant enrichment of citrate (fig. S5B). To investigate whether mitochondrial metabolism was required for conversion of glucose carbon to lipids in *ACLY*-KOs, we treated cells with the mitochondrial pyruvate carrier (MPC) inhibitor UK5099 [acyano-(1-phenylindol-3-yl)-acrylate]. MPC treatment significantly decreased fatty acid synthesis and lipogenic acetyl-CoA labeling in A549 WT cells (fig. S5, E and F), but we observed no effect in *ACLY*-KO cells. Moreover, MPC inhibition increased the relative contribution of glucose to palmitate-directed acetyl-CoA (fig. S5, E and F), further suggesting that mitochondrial pyruvate metabolism is not contributing significantly to palmitate synthesis in these *ACLY*-KO A549 cells. Likewise, ^{13}C pyruvate and glutamine also yielded negligible label on palmitate in A549 *ACLY/ACSS2*-DKO cells (Fig. 5, B to D), suggesting that ACSS2 is involved in the conversion of pyruvate to acetyl-CoA (Fig. 5A). Such a mechanism has been described whereby reactive oxygen species facilitate oxidative decarboxylation of pyruvate to acetate (*50*). The combination of KO cells and tracers applied here suggests that this activity supports acetyl-CoA generation, but the extracellular acetate, ACSS2, and lipid dependency of *ACLY*-KO cell growth suggests that this de novo acetate flux is not significant enough to sustain

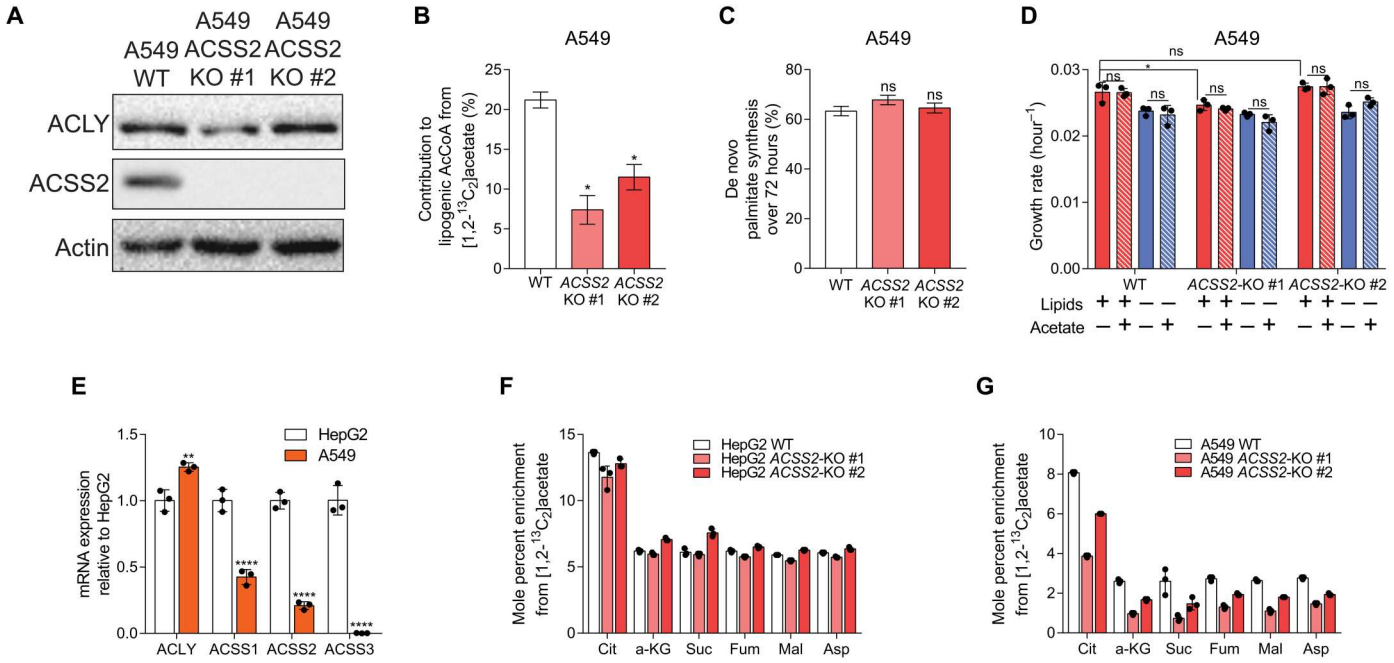

Fig. 3. ACSS2-KO attenuates catabolism of exogenous acetate with minimal effect on glucose catabolism. (**A**) Western blots of ACLY, ACSS2, and actin in A549 WT and ACSS2-KO cells. (**B**) Percent of lipogenic acetyl-CoA contributed by [1,2-13C2] acetate based on ISA modeling in A549 ACSS2-KO cells cultured in high-glucose DMEM + 10% dFBS + 1 mM acetate for 24 hours ($n = 3$). (**C**) De novo synthesis of palmitate in A549 ACSS2-KO cells cultured in high-glucose DMEM + 10% dFBS for 72 hours ($n = 3$). (**D**) Growth rates of A549 WT and ACSS2-KO cells grown in high-glucose DMEM + 10% dFBS or delipidated dFBS ± 1 mM acetate for 4 days ($n = 3$). (**E**) mRNA expression of acetyl-CoA–generating enzymes in HepG2 and A549 cells ($n = 3$). (**F**) Mole percent enrichment of TCA intermediates from [1,2-13C2] acetate in HepG2 ACSS2-KO cells cultured in high-glucose DMEM + 10% dFBS + 1 mM acetate for 24 hours ($n = 3$). (**G**) Mole percent enrichment of TCA intermediates from [1,2-13C2] acetate in A549 ACSS2-KO cells cultured in high-glucose DMEM + 10% dFBS + 1 mM acetate for 24 hours ($n = 3$). In (B) and (C), *data are plotted as mean estimated flux ± 95% confidence intervals generated via parameter continuation in INCA. In (D) to (G), data are plotted as means ± SD. Statistical significance is determined by two-way ANOVA with Tukey's method for multiple comparisons (D) or relative to HepG2 as determined by two-sided Student's *t* test (G) with $^*P < 0.05$, $^{**}P < 0.01$, and $^{****}P < 0.0001$. Unless indicated, all data represent biological triplicates. Data shown are from one of at least two separate experiments. See also Figure S3.

the biosynthetic needs of the ACLY-deficient cells tested here (Fig. 2C and fig. S2C).

To examine how oxidation of fatty acyl-CoA might contribute to acetyl-CoA homeostasis, we traced the A549 cell panel with 500 μM [U-$^{13}C_8$]octanoate, which passively diffuses across the mitochondrial membrane as well as peroxisomal membranes (*39*). Notably, octanoate contributed significantly to fatty acid biosynthesis, even in *ACLY/ACSS2*-DKO cells (Fig. 5, E and F, and fig. S5C) and contrasting results with glucose, acetate, or glutamine tracers (Figs. 4, C and D, and 5D). *ACLY*-KO and *ACLY/ACSS2*-DKO cells had a 2.5- and 4-fold increase, respectively, in enrichment of the lipogenic acetyl-CoA pool from octanoate compared to the WT or *ACSS2*-KO cells (Fig. 5E). Similar trends in lipogenic acetyl-CoA labeling from [U-$^{13}C_8$]octanoate were observed in HepG2 and 634T *ACLY*-KO clones (fig. S5C). Supplementation of octanoate enabled quantitation of fractional new fatty acid synthesis in *ACLY/ACSS2*-DKO cells by ISA (Fig. 5F). Citrate enrichment from octanoate was also increased in the *ACLY*-KO and *ACLY/ACSS2*-DKO cells (fig. S5D). However, on the basis of the previous [U-$^{13}C_5$]glutamine tracing results (Fig. 5D), mitochondrial citrate minimally contributes to fatty acid synthesis in the *ACLY*-KO or *ACLY/ACSS2*-DKO cells, and no carnitine was added to cultures (*49*), suggesting that ACLY-deficient cells use peroxisomal metabolism to supply acetyl-CoA for biosynthesis (Fig. 5G).

Peroxisomal β-oxidation supplies lipogenic acetyl-CoA in the absence of ACLY and ACSS2

Peroxisomes are the site of β-oxidation for VLCFAs and BCFAs. Peroxisomes are closely associated with lipid droplets and contain the metabolic machinery for acetyl-CoA generation from diverse fatty acids (*51*). Izzo *et al.* (*49*) observed increased expression of peroxisomal fatty acid oxidation genes in their *ACLY/ACSS2*-DKO cell lines. To test whether peroxisomes could serve as an appreciable source of acetyl-CoA in cancer cells, we profiled lipid abundances in the A549 cell panel. While total TAGs were slightly reduced in most cells, total PCs were unchanged (Fig. 6A). However, we detected significant alterations in the acyl-chain composition of the lipids, such that TAGs and PCs containing VLCFAs were depleted in *ACLY*-KO and *ACLY/ACSS2*-DKO cells (Fig. 6, B and C). This depletion is complete for nearly all measurable VLCFA containing saturated, mono-, and di-unsaturated TAG species (fig. S6A) as well as saturated and mono-unsaturated PC species (fig. S6B). Depletion of VLCFAs in lipids suggests altered VLCFA homeostasis, potentially due to increased VLCFA oxidation in the peroxisome or decreased elongation using acetyl-CoA.

To further investigate, we studied role of peroxisomes in noncanonical lipogenic acetyl-CoA contribution. Peroxisome maintenance depends on the import of nuclear-encoded proteins containing a peroxisomal targeting signal 1, which are recognized by cytosolic PEX5 receptors that transport them into the

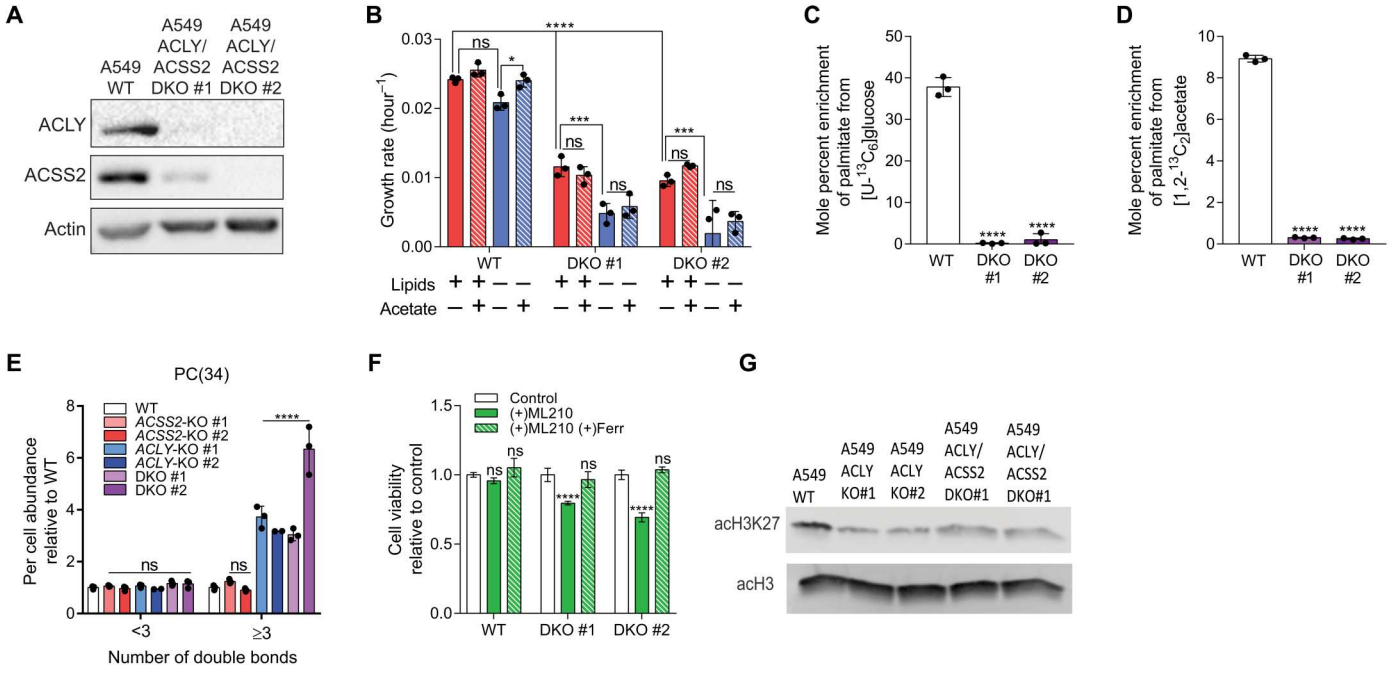

Fig. 4. ACLY/ACSS2-DKO cells are reliant on extracellular lipids, with minimal change in protein acetylation. (**A**) Western blots of ACLY, ACSS2, and actin in A549 WT and ACLY/ACSS2-DKO cells. (**B**) Growth rates of A549 WT and ACLY/ACSS2-DKO cells grown in high-glucose DMEM + 10% dFBS or delipidated dFBS ± 1 mM acetate for 4 days ($n = 3$). (**C**) Mole percent enrichment of palmitate from [U-13C6] glucose in A549 ACLY/ACSS2-DKO cells cultured in high-glucose DMEM + 10% dFBS for 72 hours ($n = 3$). (**D**) Mole percent enrichment of palmitate from [1,2-13C2] acetate in A549 ACLY/ACSS2-DKO cells cultured in high-glucose DMEM + 10% dFBS + 1 mM acetate for 24 hours ($n = 3$). (**E**) PC(34) abundance of A549 WT, ACSS2-KO, ACLY-KO, and ACLY/ACSS2-DKO cells cultured in high-glucose DMEM + 10% FBS for 2 days ($n = 3$). (**F**) Cell viability of A549 WT and ACLY/ACSS2-DKO cells cultured in DMEM + 10% dFBS ± 2 μM ML210 and/or 2 μM ferrostatin for 48 hours ($n = 4$). (**G**) Acid-extracted histone Western blot from A549 WT, ACLY-KO, and ACLY/ACSS2 DKO cells cultured in DMEM + 10% FBS 24 hours ($n = 3$). In (B) to (F), data are plotted as means ± SD. Statistical significance is determined by two-way ANOVA with Tukey's method for multiple comparisons (B) or relative to WT as determined by one-way ANOVA with Dunnet's method for multiple comparisons (C) to (F) with $^*P < 0.05$, $^{***}P < 0.001$, and $^{****}P < 0.0001$. Unless indicated, all data represent biological triplicates. Data shown are from one of at least two separate experiments. See also Figure S4.

peroxisomal lumen. In the absence of PEX5 peroxisomal enzyme, transport is ablated and metabolism is altered (*52*). To further investigate the role of peroxisomes in supporting acetyl-CoA metabolism, we generated *PEX5* and *ACLY/PEX5*-knockout (*ACLY/PEX5*-KO) clones using CRISPR-Cas9 in A549 cells (Fig. 6D). *ACLY/ACSS2/PEX5* triple knockout cells did not proliferate and could not be tested. We then cultured A549 *PEX5*-KO cells with 500 μM [U-$^{13}C_8$]octanoate and quantified its contribution to the lipogenic acetyl-CoA pool. Intriguingly, both enrichment from octanoate and fatty acid synthesis were significantly lower in *ACLY/PEX5*-KO cells compared to *ACLY*-KO cells (Fig. 6, E and F), providing evidence that peroxisomal metabolism supports acetyl-CoA and lipid synthesis. On the other hand, we saw no effect of PEX5 deficiency on lipogenic acetyl-CoA enrichment or palmitate synthesis in WT cells (Fig. 6, E and F). The labeling distribution of palmitate from [U-$^{13}C_8$]octanoate highlights these changes, as *ACLY*-KO cells showed robust incorporation but *ACLY/PEX5*-KO cells showing predominantly M8 palmitate (or direct incorporation of octanoate; fig. S6C). These data suggest that knockout of PEX5 disrupts the contribution of peroxisomal fatty acid oxidation to lipogenic acetyl-CoA production in the ACLY-KO cells (Fig. 6G). We also observed a decrease in octanoate-mediated histone acetylation in *ACLY/PEX5*-KOs compared to *ACLY*-KO cells in delipidated media (fig. S6D). To further support peroxisomal oxidation in *ACLY*-KO cells, we traced with long-chain fatty acid [U-$^{13}C_{18}$] oleate (*38*). We observed an increase in lysophosphatidylcholine (LPC) 16:1 enrichment from [U-$^{13}C_{18}$]oleate in *ACLY* KO cells compared to WT A549 cells, indicating increased reliance on exogenous fatty acid oxidation (Fig. 6H). As expected in *ACLY/PEX5* KOs, LPC 16:1 enrichment from [U-$^{13}C_{18}$]oleate decreased (Fig. 6H).

To elucidate how impairing peroxisomal β-oxidation affects proliferation of cells lacking ACLY, we quantified the growth of each cell line in response to knockout of *PEX5*. Notably, *ACLY/PEX5*-KO cells showed a significant decrease in growth relative to *ACLY*-KO cells, whereas there was no growth effect on single *PEX5*-KO cells compared to WT (Fig. 6I). Last, we quantified the growth of entire A549 ACLY/ACSS2-KO cell panel in response to increasing concentrations of the peroxisomal β-oxidation inhibitor, thioridazine (Thio) (*53*, *54*). Notably, *ACLY*-KO and *ACLY/ACSS2*-DKO cells were significantly more sensitive to Thio treatment than WT or *ACSS2*-KO cells (fig. S6E). Application of 2.5 μM Thio had no appreciable impact on growth of WT and *ACSS2*-KO cells but significantly decreased proliferation of *ACLY*-KO and *ACLY/ACSS2*-DKO cells (Fig. 6J). Together, these results suggest that peroxisomal β-oxidation provides a significant growth sustaining level of acetyl-CoA in the absence of functional ACLY. Multiple mechanisms have been suggested for shuttling peroxisomal acetyl-CoA to the cytosol in mammalian cells, including conversion to acetate by a thioesterase and subsequent export (and activation by ACSS2 in the

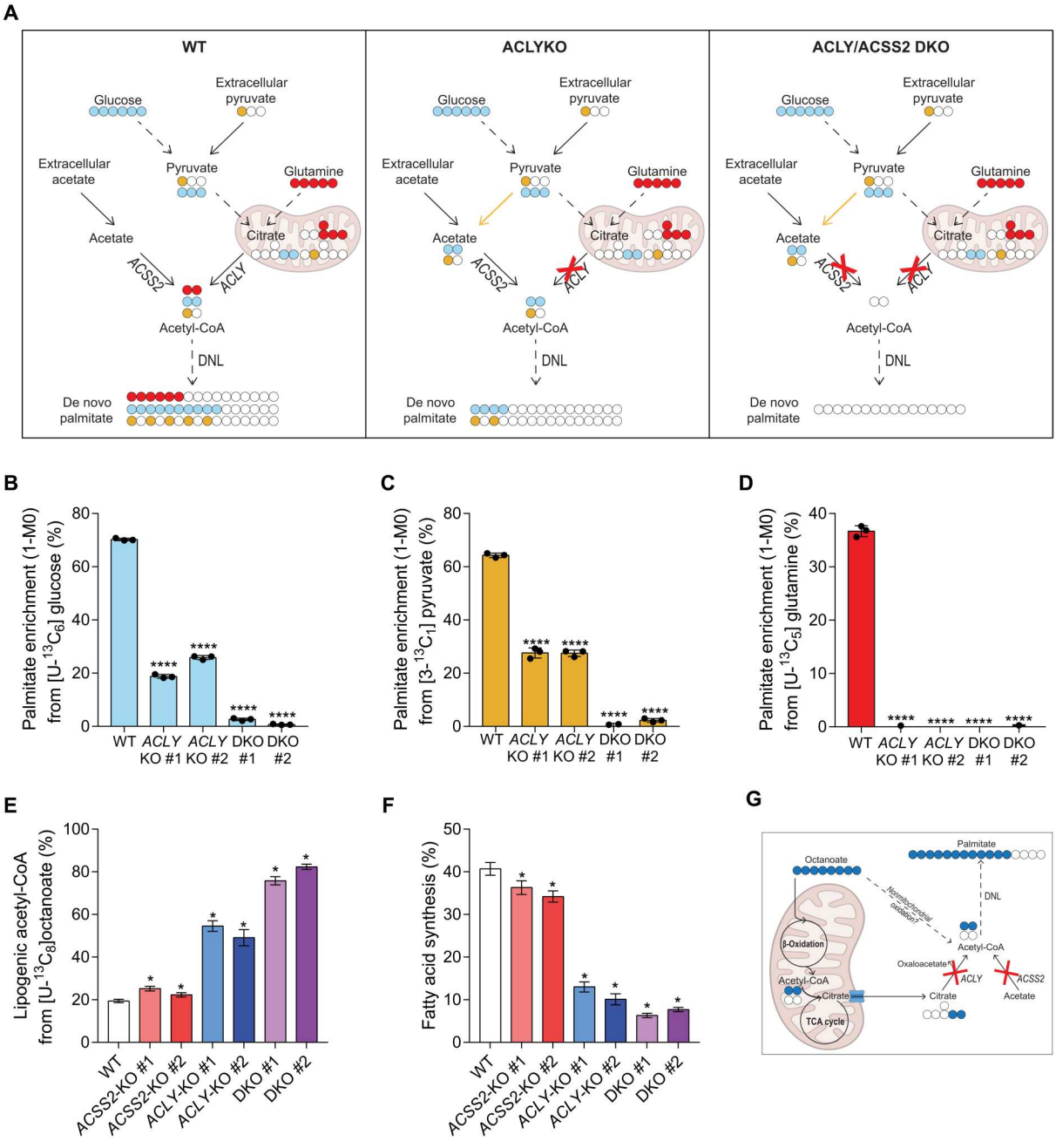

Fig. 5. Disruption of canonical acetyl-CoA synthesis induces alternative synthesis pathways. (**A**) Schematic showing de novo acetate synthesis in ACLY-KO cells. Dashed lines represent multiple reactions. (**B**) Enrichment (1-M0) of palmitate from [U-13C6] glucose in A549 WT, ACLY-KO, and ACLY/ACSS2-DKO cells cultured in high-glucose DMEM + 10% dFBS for 72 hours ($n = 3$). (**C**) Enrichment (1-M0) of palmitate from [3-13C1] pyruvate in A549 WT, ACLY-KO, and ACLY/ACSS2-DKO cells cultured in high-glucose DMEM + 10% dFBS + 5 mM pyruvate for 72 hours ($n = 3$). (**D**) Enrichment (1-M0) of palmitate from [U-13C5] glutamine in A549 WT, ACLY-KO, and ACLY/ACSS2-DKO cells cultured in high-glucose DMEM + 10% dFBS for 72 hours ($n = 3$). (**E**) Percent of lipogenic acetyl-CoA contributed by [U-13C8]octanoate based on ISA modeling in A549 WT, ACSS2-KO, ACLY-KO, and ACLY/ACSS2-DKO cells cultured in high-glucose DMEM + 10% dFBS + 500 μM octanoate for 24 hours ($n = 3$). (**F**) De novo synthesis of palmitate in A549 WT, ACSS2-KO, ACLY-KO, and ACLY/ACSS2-DKO cells cultured in high-glucose DMEM + 10% dFBS + 500 μM octanoate for 24 hours ($n = 3$). (**G**) Schematic of nonmitochondrial acetyl-CoA synthesis from [U-13C8]octanoate in ACLY/ACSS2-DKO cells. Filled circles are 13C, and empty circles are 12C. In (B) to (F), data are plotted as means ± SD. Statistical significance relative to WT as determined by one-way ANOVA with Dunnet's method for multiple comparisons (B) to (D) with $^*P < 0.05$, $^{**}P < 0.01$, $^{***}P < 0.001$, and $^{****}P < 0.0001$. In (E) and (F), *data are plotted as mean estimated flux ± 95% confidence intervals generated via parameter continuation in INCA. Unless indicated, all data represent biological triplicates. Data shown are from one of at least two separate experiments. See also fig. S5.

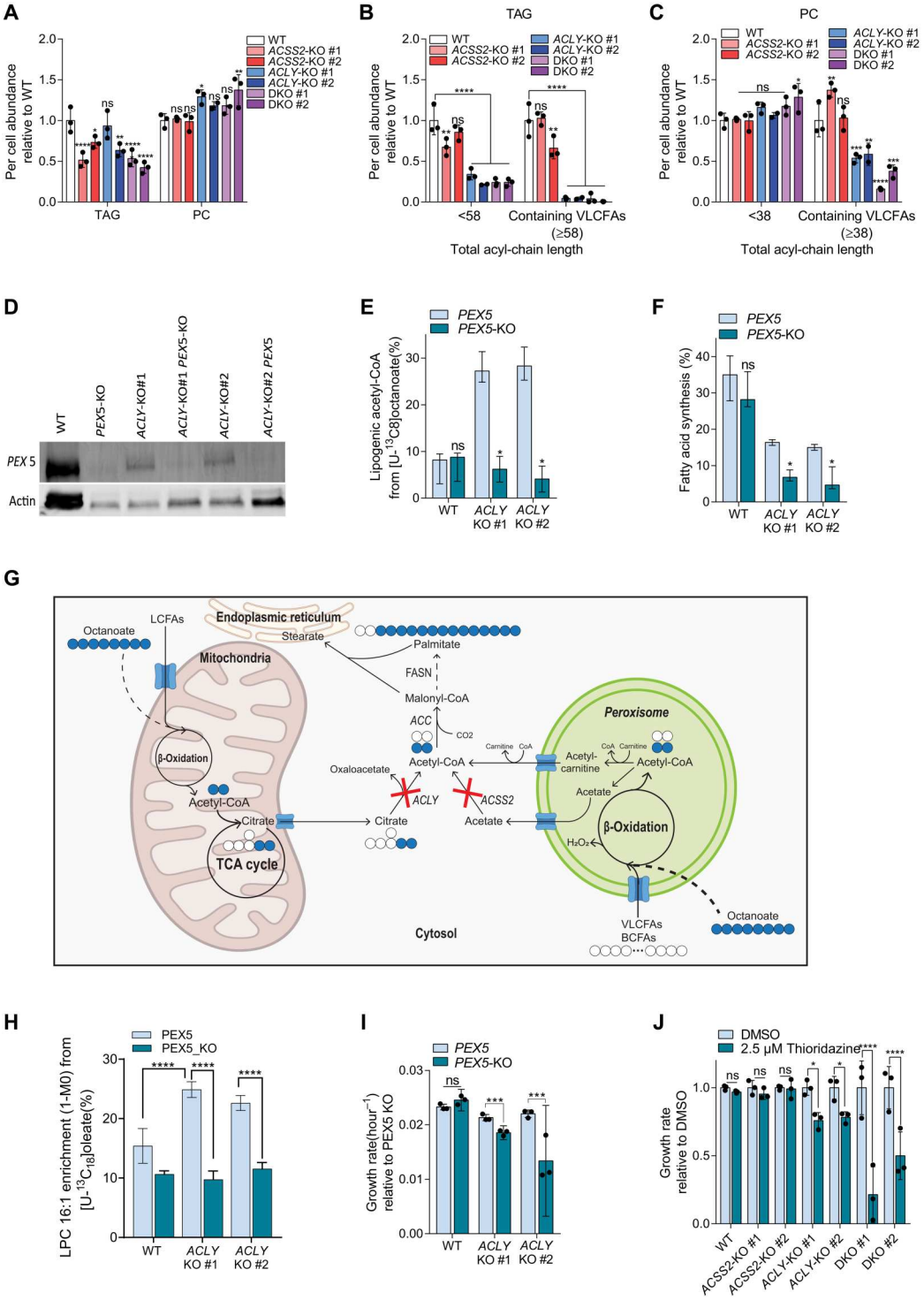

Fig. 6. Peroxisomal β-oxidation becomes a major source of lipogenic acetyl-CoA with ACLYKO and ACLY/ACSS2 DKO. (**A** to **C**) Total abundance of TAGs and PCs (A), total abundance of saturated, mono- and di-unsaturated TAGs per cell (B), and total abundance of saturated and monounsaturated PCs per cell (C) in A549 WT, ACSS2-KO, ACLY-KO, and ACLY/ACSS2-DKO cells cultured in high-glucose DMEM + 10% FBS for 2 days (n = 3). (**D**) Western blots of PEX5 and actin in A549 WT, PEX5 KO, ACLY KO, and ACLY-PEX5-KO cells. (**E** and **F**) Percent of lipogenic acetyl-CoA contributed by [U-13C8]octanoate based on ISA modeling (E) and de novo synthesis of palmitate (F) in A549 WT, PEX5-KO, ACLY-KO, and ACLY/PEX-5 KO cells cultured in high-glucose DMEM + 10% dFBS for 48 hours (n = 3). (**G**) Schematic of peroxisomal acetyl-CoA synthesis from [U-13C8]octanoate in ACLY/ACSS2-DKO cells. Filled circles are 13C, and empty circles are 12C. (**H**) Enrichment (1-M0) of LPC from 100 μM [U-13C18] oleate in A549 WT, ACLY-KO, and ACLY/PEX5-DKO cells cultured in high-glucose DMEM + 10% dFBS for 48 hours (n = 3). (**I**) Growth rates of A549 WT and ACLY-KO relative to PEX5 KO cells grown in high-glucose DMEM + 10% FBS for 4 days. (**J**) Growth rates of A549 WT and ACLY/ACSS2-DKO cells grown in high-glucose DMEM + 10% dFBS ± 2.5 μM thioridazine (Thio) relative to DMSO for 4 days (n = 3). In (A) to (C) and (H) to (J), data are plotted as means ± SD. Statistical significance as determined by one-way ANOVA with Dunnet's method for multiple comparisons relative to WT (A to C) or DMSO (J) with *P < 0.05, **P < 0.01, ***P < 0.001, and ****P < 0.0001. In (E) and (F), data are plotted as mean ± 95% confidence interval. "*" indicates statistical significance by non-overlapping confidence intervals. Unless indicated, all data represent biological triplicates. Data shown are from one of at least two separate experiments. See also fig. S6. DMSO, dimethyl sulfoxide.

cytosol), shuttling as acetyl-carnitine facilitated by peroxisomal CRAT (*55*–*57*), or via peroxisomal coenzyme A transporters like solute carrier family 25 member 17 (Slc25a17) and ATP binding cassette subfamily D member 1 (ABCD1) (*58*–*60*). To this end, we observed a significant increase in acetyl-carnitine enrichment from [U-$^{13}C_8$]octanoate in *ACLY*-KO and *ACLY/ACSS2*-DKO cells compared to WT cells (fig. S6F), cells that are both capable of (and actually prefer) synthesizing palmitate from [U-$^{13}C_8$]octanoate (Fig. 5E). Furthermore, acetyl-carnitine enrichment from octanoate was significantly decreased in *ACLY/PEX5*-KOs (fig. S6G), providing evidence that peroxisomal metabolism supports acetyl-CoA and lipid synthesis in the absence of ACLY. Together, these metabolic tracing and knockout studies emphasize peroxisomal oxidation of exogenous lipids as a major

source of acetyl-CoA for fatty acid synthesis and histone acetylation in ACLY-deficient cells, highlighting a role for inter-organelle cross-talk in supporting cell survival in response to nutrient fluctuations.

DISCUSSION

While the core metabolic machinery of cancer cells acts "as advertised" under nutrient replete conditions, the diverse stresses experienced the tumor microenvironment induce complex rewiring of metabolic fluxes between organelles, including mitochondria, the ER, peroxisomes, and the plasma membrane. Here, we show that this organelle cross-talk is critical for cancer cells to maintain acetyl-CoA homeostasis and metabolic resilience when organelle-specific pathways become compromised. Acetyl-CoA serves as a substrate regulating numerous processes across mitochondria, the nucleus, peroxisomes, the ER, and plasma membrane but cannot cross membranes. Hence, understanding how acetyl-groups are shuttled throughout the cell for bioenergetics, biosynthesis, and cellular regulation is critically important. Here, we applied metabolic tracing and lipogenesis studies to cancer cell lines where key pathways for acetyl-CoA generation were knocked out, including ACLY, ACSS2, and peroxisomal metabolism (PEX5). We further highlight a key role for peroxisomal metabolism in providing acetyl-CoA for fatty acid synthesis and histone acetylation in the context of ACLY deficiency.

Acetyl-CoA–fueled fatty acid synthesis is important for cancer progression in NSCLC models, whether this occurs in endogenous tissues or in situ within tumors (*7*). Targeting of ACLY to reduce tumor cell growth and increase dependence on exogenous lipids has also been explored in detail (*24*–*26*, *61*). Likewise, ACSS2 has garnered significant interest as a mechanism through which cancer cells source acetyl-CoA for growth and survival (*31*–*33*, *62*). ACSS2 expression and acetate-dependent flux both increase in the context of ACLY deficiency (*36*), and trafficking of acetate to the nucleus for histone acetylation may be an important aspect of this enzyme's function (*45*, *63*–*65*). The impact of ACSS isozyme expression on acetate shuttling, fatty acid synthesis, and epigenetic regulation warrants further study as it may provide insight into how therapeutic interventions targeting acetate catabolism affect whole body physiology. Peroxisomes further complicate these questions, particularly in reference to their impact on lipid homeostasis and diversity. Understanding how these nodes of metabolic exchange are exploited by cancer cells shed light on resistance mechanisms, as these redundancies in pathway architecture can reduce efficacy of drugs targeting metabolic enzymes (*66*).

Beyond cancer, understanding how cells manage intracellular metabolic pools using these KO and tracing approaches is also relevant for states of "overnutrition." Exogenous treatment of fatty acids or lipids to cells in vitro often occurs at supra-physiological levels, so our studies further highlight the role of peroxisomal metabolism in generating acetyl-CoA for lipid biosynthesis and acetylation (*51*). While these KO systems lack some physiology in the acute nature of pathway targeting, they also allow one to focus biochemical studies on these alternate pathways when substrate levels are high. However, we and Izzo *et al.* (*49*), in this issue, also note key questions that remain such as the relative contribution of mitochondrial versus peroxisomal oxidation and the dependence on carnitine for transport since both organelles express CRAT (*67*, *68*). Our data indicate that the mitochondrial pathway is not sufficiently active to support cell growth in these cells, suggesting a role for peroxisomes in some cells or environments where carbohydrates are deficient or mitochondria inactive (e.g., hypoxia). The relative contribution of each pathway likely shifts as a function of cell and tissue type. By understanding how these metabolic pathways are balanced, they can be more effectively targeted both in neoplastic or metabolically stressed tissues.

MATERIALS AND METHODS

Cell Lines

A549 and HepG2 cells were obtained from HDBiosciences, HAP1 cells were obtained from Horizon Discovery, and 634T cells were obtained from the Shaw Lab at the Salk Institute for Biological Sciences. All cell lines were incubated at 37°C with 5% CO_2 and cultured using Dulbecco's modified Eagle's medium (DMEM) with 10% FBS and 1% penicillin-streptomycin. Cells were tested negative for mycoplasma contamination. All media were adjusted to pH = 7.3.

Cell proliferation and ^{13}C tracing

Proliferation studies were performed on 12-well plates with an initial cell number of 50,000 per well for A549s and 100,000 per well for HepG2s. Cells were plated in growth media and allowed to adhere for 24 hours before changing to the specified growth media. Cell counts were performed at days 0 and 4 using a hemocytometer.

^{13}C isotope tracing media was formulated using glucose- and glutamine-free DMEM 5030 supplemented with either 20 mM [U-$^{13}C_6$]glucose, 4 mM [U-$^{13}C_5$]glutamine, 1 mM [1,2-$^{13}C_2$]acetate, 5 mM [3-$^{13}C_1$]pyruvate, 500 μM [U-$^{13}C_8$]octanoate, or 500 μM [2,4-$^{13}C_2$]citrate (Cambridge Isotopes) and 10% dFBS. ^{13}C oleate studies were performed with 100 μM albumin-conjugated [U-$^{13}C_{18}$] oleate and 10% dFBS. All studies were performed with a final concentration of 20 mM glucose and 4 mM glutamine. Cultured cells were washed with 1 ml of phosphate-buffered saline (PBS) before applying tracing media for 6 to 72 hours as indicated in figure legends.

Drug-dose response

Drug-dose response studies were performed on 96-well plates with an initial cell number of 2500 per well. Cells were plated in growth media and allowed to adhere for 24 hours before changing to the specified growth media with the indicated concentration of Thio. After 4 days, wells were washed two times with tap water, and 50 μl of 0.5% crystal violet staining solution was added to each well for 20 min. Crystal violet stain was removed, and wells were washed three times with tap water and air dried overnight. Next, 200 μl of methanol was added to each well, and plates were incubated at room temperature for 20 min. Optical density of wells was measured at 570 nm on a TECAN plate reader.

Ferroptosis assay

WT and ACLY/ACSS2-DKO cells were plated in 96-well plates with an initial cell number of 5000 per well. Cells were plated in growth media and allowed to adhere for 24 hours before changing to the specified growth media with 2 μM ML210 and/or 6 μM ferrostatin. After 48 hours, cell viability was quantified using the PrestoBlue

Cell Viability (Thermo Fisher Scientific, A13261) and a TECAN plate reader.

Isotopomer spectral analysis

ISA was performed to estimate the percent of newly synthesized palmitate as well as the contribution of a tracer of interest to the lipogenic acetyl-CoA pool (*69*, *70*). Parameters for contribution of ^{13}C tracers to lipogenic acetyl-CoA (*D* value) and percentage of newly synthesized fatty acid [*g*(*t*) value] and their 95% confidence intervals are then calculated using best-fit model from INCA MFA (isotopomer network compatmental analysis metabolic flux analysis) software. Experimental palmitate labeling from [U-$^{13}C_6$]glucose, [U-$^{13}C_5$]glutamine, [1,2-$^{13}C_2$]acetate, [U-$^{13}C_8$]octanoate, or [2,4-$^{13}C_2$]citrate after a 24- to 72-hour trace, as indicated in figure legends, was compared to simulated labeling using a reaction network where C16:0 is condensation of eight AcCoA. ISA data plotted as mean ± 95% confidence interval. "*" indicates statistical significance by non-overlapping confidence intervals. Reaction model and the fragment ion(s) of palmitate used in the ISA method are included in table S2.

CRISPR-Cas9–engineered knockout cell lines

HDBiosciences generated A549 and HepG2 *ACLY*-KO, *ACSS2*-KO, and *ACLY/ACSS2*-DKO cell lines. *ACLY*, *ACSS2*, and *ACLY/ACSS2* knockout clones were generated using the strategy described previously (*71*). Briefly, a tandem guide RNAs (gRNAs) was designed to target the human *ACLY* (gRNA sequences: gaccagctgatcaaacgtcg and ggggtcaggatgaacgtgtg) and *ACSS2* (gRNA sequences: ctcgcggt agcgctgcagcg and aatggaaaagggattccggg) using the online CRISPR guide tool provided by the Zhang Lab at MIT (Massachustts Institute of Technology) (https://zlab.bio/guide-design-resources). The gRNA duplex was cloned into lentiCRISPRv2 (Addgene, #52961) (*72*). A549 and HepG2 cells were transfected with the *ACLY*- and/or *ACSS2*-specific gRNA to generate pooled knockouts. After puromycin selection, single-cell clones were isolated by diluting the pooled knockout lines at 1 cell/100 μl and plating 100 μl into each well of a 96-well plate. Clones were maintained by exchanging media every 3 to 5 days. Clones were validated by polymerase chain reaction (PCR) and Western blot. PEX5 and ACLY/PEX5 knockout clones were generated using the strategy described previously (*73*). Briefly, chemically modified gRNAs (Synthego) were designed to target the human PEX5 (gRNA sequence: guugguggcugaauucc). gRNAs were complexed with recombinant Cas9 [Integrated DNA Technologies (IDT)], catalog no. 1081059) and introduced into cells by electroporation (4D-Nucleofector, Lonza Biosciences) according to the manufacturer's protocols. Single-cell clones were generated by serial dilution of the bulk knockout population in 96-well plates. Clones were maintained by exchanging the media every 3 days and validated by Western blot.

Lentivirus production

One 10-cm dish of human embryonic kidney–293FT cells at 60% confluency was transfected with 1.3 μg of VSV.G/pMD2.G, 5.3 μg of lenti-gag/pol/pCMVR8.2, and 4 μg of the gRNA duplexed lenti-CRISPRv2 using 16 μl of Lipofectamine 3000 diluted in 0.66 ml of OPTI-MEM. Medium containing viral particles was harvested 48 and 72 hours after transfection, then concentrated by Centricon Plus-20 100,000 nominal molecular weight limit (NMWL) centrifugal ultrafilters, divided into aliquots, and frozen at −80°C.

Metabolic flux analysis

Metabolic fluxes for citrate were calculated by collecting media at time 0 and spent media after 72 hours. Spent media was centrifuged at 300*g* for 5 min, to remove cell debris. Cell counts were performed at time 0 and after 72 hours as well.

Metabolite extraction and GC-MS analysis

At the conclusion of the tracer experiment, media was aspirated. Then, cells were rinsed twice with 0.9% saline solution and lysed with 250 μl of ice-cold methanol. After 1 min, 100 μl of water containing norvaline (1 μg/ml) was added to each sample and vortexed for 1 min. Two hundred fifty microliters of chloroform was added to each sample, and all were vortexed again for 1 min. After centrifugation at 21,130*g* for 10 min at 4°C, 250 μl of the upper aqueous layer was collected and evaporated under vacuum at 4°C. Then, 250 μl of the lower organic layer was collected and evaporated under air at room temperature. Dried polar and nonpolar metabolites were processed for gas chromatography–mass spectrometry (GC-MS) as described previously by Cordes and Metallo (*70*). Briefly, polar metabolites were derivatized using a Gerstel MultiPurpose Sampler (MPS 2XL). Methoxime–*tert*-butyldimethylchlorosilane (tBDMS) derivatives were formed by addition of 15 μl of 2% (w/v) methoxylamine hydrochloride (MP Biomedicals, Solon, OH) in pyridine and incubated at 45°C for 60 min. Samples were then silylated by addition of 15 μl of *N*-*tert*-butyldimethylsily-*N*-methyltrifluoroacetamide (MTBSTFA) with 1% tBDMS (Regis Technologies, Morton Grove, IL) and incubated at 45°C for 30 min. Nonpolar metabolites were saponified and transesterified to fatty acid methyl esters (FAMEs) by adding 500 μl of 2% H_2SO_4 in methanol to the dried nonpolar layer and heating at 50°C for 1 hour. FAMEs were then extracted by adding 100 μl of a saturated salt solution and 500 μl of hexane and vortexing for 1 min. The hexane layer was removed, evaporated, and resuspended with 60 μl of hexane for injection.

Derivatized polar samples were injected into a GC-MS using a DB-35MS column (30 m by 0.25 mm i.d. by 0.25 μm; Agilent J&W Scientific, Santa Clara, CA) installed in an Agilent 7890B GC system integrated with an Agilent 5977a MS. Samples were injected at a GC oven temperature of 100°C which was held for 1 min before ramping to 255°C at 3.5°C/min and then to 320°C at 15°C/min and held for 3 min. Electron impact ionization was performed with the MS scanning over the range of 100 to 650 mass/charge ratio (*m*/*z*) for polar metabolites.

Derivatized nonpolar samples were injected into a GC-MS using a FAME Select column (100 m by 0.25 mm i.d. by 0.25 μm; Agilent J&W Scientific, Santa Clara, CA) installed in an Agilent 7890A GC system integrated with an Agilent 5977A MS. Samples were injected at a GC oven temperature of 80°C which was held for 1 min before ramping to 170°C at 20°C/min, then to 188°C at 1°C/min, and then to 250°C at 20°C/min and held for 10 min. Electron impact ionization was performed with the MS scanning over the range of 54 to 400 *m*/*z* for nonpolar metabolites.

Metabolite levels and mass isotopomer distributions were analyzed with an in-house MATLAB script which integrated the metabolite fragment ions and corrected for natural isotope

abundances. Mole percent enrichment calculations were performed using Escher-Trace (*74*).

LC-MS/MS analysis

Lipids were extracted from confluent six-well plates after growth in DMEM + 10% FBS + 1% penicillin streptomycin for 48 hours. At the conclusion of the experiment, media was aspirated, and the cells were rinsed twice with saline solution. Cells were lysed with 750 μl of ice cold 1:1 methanol/water solution for 5 min on ice and scraped into Eppendorf tubes. Next, 500 μl of ice cold chloroform and 50 μl of butylated hydroxytoluene (1 mg/ml in methanol) were added to the tube, along with EquiSLASH (Avanti, Croda International Plc, 330731internal standard). The tubes were vortexed for 5 min and centrifuged at 21,230*g* at 4°C for 5 min. The lower organic phase was collected, and 2 μl of formic acid was added to the remaining polar phase which was re-extracted with 500 μl of chloroform. Combined organic phases were dried under nitrogen, and the pellet was resuspended in 50 μl of isopropyl alcohol.

A Q Exactive orbitrap mass spectrometer with a Vanquish Flex Binary UHPLC (ultra-high-performance liquid chromatography) system (Thermo Fisher Scientific) was used with an Accucore C30, 150 by 2.1 mm, 2.6-μm particle (Thermo Fisher Scientific) column at 40°C. Five microliters of sample was injected. Chromatography was performed using a gradient of 40:60 (v/v) water:acetonitrile with 10 mM ammonium formate and 0.1% formic acid (mobile phase A) and 10:90 (v/v) acetonitrile: 2-propanol with 10 mM ammonium formate and 0.1% formic acid (mobile phase B), both at a flow rate of 0.2 ml/min. The LC gradient ran from 30 to 43% B from 3 to 8 min, then from 43 to 50% B from 8 to 9 min, then 50 to 90% B from 9 to 18 min, and then 90 to 99% B from 18 to 26 min and then held at 99% B from 26 to 30 min, before returning to 30% B in 6 min and held for a further 4 min.

Lipids were analyzed in positive mode using spray voltage 3.2 kV. Sweep gas flow was 1 arbitrary units, auxiliary gas flow was 2 arbitrary units, and sheath gas flow was 40 arbitrary units, with a capillary temperature of 325°C. Full MS (scan range, 200 to 2000 *m/z*) was used at 70,000 resolution with 1×10^6 automatic gain control and a maximum injection time of 100 ms. Data-dependent MS2 (Top 6) mode at 17,500 resolution with automatic gain control set at 1×10^5 with a maximum injection time of 50 ms was used. Data were analyzed using EI-Maven and Escher-Trace software, and peaks were normalized to Avanti EquiSPLASH internal standard. Lipid species–specific fragments used for identification and quantitation are presented in table S1.

For acetyl carnitine measurement, polar phase was dried under air, and the pellet was resuspended in 50 μl of acetonitrile and loaded onto a Q Exactive orbitrap mass spectrometer with a Vanquish Flex Binary UHPLC system (Thermo Fisher Scientific) that was used with an iHILIC-(P) Classic, 150 by 2.1 mm, 5-μm particle, 200 Å (Hilicon) column at 45°C. Five microliters of sample was injected. Chromatography was performed using a gradient of 20 mM ammonium carbonate, adjusted to pH 9.4 with 0.1% ammonium hydroxide (25%) solution (mobile phase A) and 100% acetonitrile (mobile phase B), both at a flow rate of 0.2 ml/min. The LC gradient ran linearly from 80 to 20% B from 2 to 17 min and then from 20 to 80% B from 17 to 18 min and then held at 80% B from 18 to 25 min.

Western blot

A549, HepG2, HAP1, and 634T WT, ACLY and/or ACSS2-KO cell lines were lysed in mammalian protein extraction reagent (M-PER) buffer (Thermo Fisher Scientific, 78501) with 1× protease inhibitor (Sigma-Aldrich). Protein concentrations were determined using a Pierce BCA protein assay kit (Thermo Fisher Scientific, 23225). Fifteen micrograms of protein was loaded and separated using 4 to 15% Mini-PROTEAN TGX Precast SDS-PAGE Gels (Bio-Rad, #4561086). Samples were then transferred to nitrocellulose membranes for immunoblotting. Total acetylated-lysine (Cell Signaling Technology, 9441), β-actin (Sigma-Aldrich, A5441), ACLY (Cell Signaling Technology, 13390), ACSS2 (Cell Signaling Technology, 3658), and PEX5(D7V4D) (Cell Signaling Technology, 83020) antibodies were used to probe their respective targets. Anti-rabbit horseradish peroxidase–conjugated secondary antibodies (Millipore, AP132P) were used for imaging.

Acid extraction of histones

Cells were washed with ice-cold PBS and lysed with NIB-250 buffer [15 mM tris-HCl (pH 7.5), 5 mM $MgCl_2$, 15 mM NaCl, 60 mM KCl, 1 mM $CaCl_2$, 1 mM dithiothreitol, 250 mM sucrose, 10 mM sodium butyrate, and protease inhibitors] with 0.1% NP-40 incubate on ice for 5 min. Nuclei were pelleted at 600*g* for 5 min at 4°C. Wash nuclei were pelleted gently with 150 μl of NIB-250 without NP-40. The extracted nuclei were resuspended with 0.4 N H_2SO_4, rotated for 4 hours or overnight at 4°C to extract histone proteins, and then centrifuged at 11,000*g* at 4°C for 10 min. TCA (100%) with a final concentration of 20% was added slowly to the clarified histone extracts. Let this mixture precipitate on ice for at least 1 hour or as long as overnight. Precipitated histones were centrifuged at 11,000*g* at 4°C for 10 min. Histones were washed with 1 ml of acetone + 0.1% 12 N of HCl once and 1 ml of acetone twice. The histone pellet was air-dried at room temperature and then resuspended in glass-distilled H_2O. Resuspended histones were used for Western blotting.

RNA isolation and quantitative RT-PCR

Total RNA was purified from cultured cells using TRIzol Reagent (Life Technologies) per manufacturer′s instructions. First-strand cDNA was synthesized from 1 μg of total RNA using iScript Reverse Transcription Supermix for RT-PCR (Bio-Rad Laboratories) according to the manufacturer′s instructions. Individual 20 μl of SYBR Green real-time PCR reactions consisted of 1 μl of diluted cDNA, 10 μl of SYBR Green Supermix (Bio-Rad), and 1 μl of each 5 μM forward and reverse primers. For standardization of quantification, 18*S* was amplified simultaneously. The PCR was carried out on 96-well plates on a CFX Connect Real time System (Bio-Rad), using a three-stage program provided by the manufacturer: 95°C for 3 min, 40 cycles of 95°C for 10 s, and 60°C for 30 s. Gene-specific primers are tabulated in table S1.

Quantification and statistical analysis

Statistical analyses were performed using Graphpad Prism. Unless indicated, all results shown as means ± SD of cellular triplicates obtained from one representative experiment as specified in each figure legend. *P* values were calculated using a Student′s two-tailed *t* test, one-way analysis of variance (ANOVA) with Dunnet′s method for multiple comparisons, or two-way ANOVA with Tukey′s method for multiple comparisons; $^*P < 0.05$, $^{**}P$

<0.01, ***$P < 0.001$, and ****$P < 0.0001$. Unless indicated, all normalization and statistical tests compared to WT cells.

Supplementary Materials

This PDF file includes:

Figs. S1 to S6
Tables S1 and S2

View/request a protocol for this paper from *Bio-protocol*.

REFERENCES AND NOTES

1. J. A. Menendez, R. Lupu, Fatty acid synthase and the lipogenic phenotype in cancer pathogenesis. *Nat. Rev. Cancer* **7**, 763–777 (2007).
2. Y. Cai, J. Crowther, T. Pastor, L. A. Asbagh, M. F. Baietti, M. De Troyer, I. Vazquez, A. Talebi, F. Renzi, J. Dehairs, J. V. Swinnen, A. A. Sablina, Loss of chromosome 8p governs tumor progression and drug response by altering lipid metabolism. *Cancer Cell* **29**, 751–766 (2016).
3. M. Knobloch, S. M. G. Braun, L. Zurkirchen, C. Von Schoultz, N. Zamboni, M. J. Arauzo-bravo, W. J. Kovacs, Ö. Karalay, R. A. C. Machado, M. Roccio, M. P. Lutolf, C. F. Semenkovich, S. Jessberger, Metabolic control of adult neural stem cell activity by Fasn-dependent lipogenesis. *Nature* **493**, 226–230 (2013).
4. T. M. Loftus, D. E. Jaworsky, G. L. Frehywot, C. A. Townsend, G. V. Ronnett, M. D. Lane, F. P. Kuhajda, Reduced food intake and body weight in mice treated with fatty acid synthase inhibitors. *Science* **288**, 2379–2382 (2000).
5. J. A. Menendez, L. Vellon, I. Mehmi, B. P. Oza, S. Ropero, R. Colomer, R. Lupu, Inhibition of fatty acid synthase (FAS) suppresses HER2/neu (erbB-2) oncogene overexpression in cancer cells. *Proc. Natl. Acad. Sci. U.S.A.* **101**, 10715–10720 (2004).
6. E. S. Pizer, J. Thupari, W. F. Han, M. L. Pinn, F. J. Chrest, G. L. Frehywot, C. A. Townsend, F. P. Kuhajda, Malonyl-coenzyme-A is a potential mediator of cytotoxicity induced by fatty-acid synthase inhibition in human breast cancer cells and xenografts. *Cancer Res.* **60**, 213–218 (2000).
7. R. U. Svensson, S. J. Parker, L. J. Eichner, M. J. Kolar, M. Wallace, S. N. Brun, P. S. Lombardo, J. L. Van Nostrand, A. Hutchins, L. Vera, L. Gerken, J. Greenwood, S. Bhat, G. Harriman, W. F. Westlin, H. J. Harwood, A. Saghatelian, R. Kapeller, C. M. Metallo, R. J. Shaw, Inhibition of acetyl-CoA carboxylase suppresses fatty acid synthesis and tumor growth of non-small-cell lung cancer in preclinical models. *Nat. Med.* **22**, 1108–1119 (2016).
8. K. E. Wellen, G. Hatzivassiliou, U. M. Sachdeva, T. V. Bui, J. R. Cross, C. B. Thompson, ATP-citrate lyase links cellular metabolism to histone acetylation. *Science* **324**, 1076–1080 (2009).
9. J. V. Lee, A. Carrer, S. Shah, N. W. Snyder, S. Wei, S. Venneti, A. J. Worth, Z. F. Yuan, H. W. Lim, S. Liu, E. Jackson, N. M. Aiello, N. B. Haas, T. R. Rebbeck, A. Judkins, K. J. Won, L. A. Chodosh, B. A. Garcia, B. Z. Stanger, M. D. Feldman, I. A. Blair, K. E. Wellen, Akt-dependent metabolic reprogramming regulates tumor cell Histone acetylation. *Cell Metab.* **20**, 306–319 (2014).
10. S. Sivanand, S. Rhoades, Q. Jiang, J. V. Lee, J. Benci, J. Zhang, S. Yuan, I. Viney, S. Zhao, A. Carrer, M. J. Bennett, A. J. Minn, A. M. Weljie, R. A. Greenberg, K. E. Wellen, Nuclear acetyl-CoA production by ACLY promotes homologous recombination. *Mol. Cell* **67**, 252–265.e6 (2017).
11. H. F. Yancy, J. A. Mason, S. Peters, C. E. Thompson III, G. K. Littleton, M. Jett, A. A. Day, Metastatic progression and gene expression between breast cancer cell lines from African American and Caucasian women. *J. Carcinog.* **6**, 8 (2007).
12. E. D. Pope III, E. O. Kimbrough, L. P. Vemireddy, P. K. Surapaneni, J. A. Copland III, K. Mody, Aberrant lipid metabolism as a therapeutic target in liver cancer. *Expert Opin. Ther. Targets* **23**, 473–483 (2019).
13. J. Turyn, B. Schlichtholz, A. Dettlaff-Pokora, M. Presler, E. Goyke, M. Matuszewski, Z. Kmieć, K. Krajka, J. Swierczynski, Increased activity of glycerol 3-phosphate dehydrogenase and other lipogenic enzymes in human bladder cancer. *Horm. Metab. Res.* **35**, 565–569 (2003).
14. A. Varis, M. Wolf, O. Monni, M.-L. Vakkari, A. Kokkola, C. Moskaluk, H. Frierson Jr., S. M. Powell, S. Knuutila, A. Kallioniemi, W. El-rifai, Targets of gene amplification and overexpression at 17q in Gastric cancer. *Cancer Res.* **62**, 2625–2629 (2002).
15. Y. Zhou, L. R. Bollu, F. Tozzi, X. Ye, R. Bhattacharya, G. Gao, E. Dupre, L. Xia, J. Lu, F. Fan, S. Bellister, L. M. Ellis, Z. Weihua, ATP citrate lyase mediates resistance of colorectal cancer cells to SN38. *Mol. Cancer Ther.* **12**, 2782–2791 (2013).
16. M. E. Beckner, W. Fellows-Mayle, Z. Zhang, N. R. Agostino, J. A. Kant, B. W. Day, I. F. Pollack, Identification of ATP citrate lyase as a positive regulator of glycolytic function in glioblastomas. *Int. J. Cancer* **126**, 2282–2295 (2011).
17. T. Migita, T. Narita, K. Nomura, E. Miyagi, F. Inazuka, M. Matsuura, M. Ushijima, T. Mashima, H. Seimiya, Y. Satoh, S. Okumura, K. Nakagawa, Y. Ishikawa, ATP citrate lyase: Activation and therapeutic implications in non–small cell lung cancer. *Cancer Res.* **68**, 8547–8554 (2008).
18. X. Qian, J. Hu, J. Zhao, H. Chen, ATP citrate lyase expression is associated with advanced stage and prognosis in gastric adenocarcinoma. *Int. J. Clin. Exp. Med.* **8**, 7855–7860 (2015).
19. C. Sullivan, J. G. Hamilton, R. Wheatley, C. River, B. Laboratories, Inhibition of lipogenesis in rat liver by (−)-hydroxycitrate. *Arch. Biochem. Biophys.* **150**, 183–190 (1972).
20. J. M. Lowenstein, Effect of (−)-hydroxycitrate on fatty acid synthesis by rat liver in vivo. *J. Biol. Chem.* **246**, 629–632 (1971).
21. S. L. Pinkosky, S. Filippov, R. A. K. Srivastava, J. C. Hanselman, C. D. Bradshaw, T. R. Hurley, C. T. Cramer, M. A. Spahr, A. F. Brant, J. L. Houghton, C. Baker, M. Naples, K. Adeli, R. S. Newton, AMP-activated protein kinase and ATP-citrate lyase are two distinct molecular targets for ETC-1002, a novel small molecule regulator of lipid and carbohydrate metabolism. *J. Lipid Res.* **54**, 134–151 (2013).
22. D. E. Bauer, G. Hatzivassiliou, F. Zhao, C. Andreadis, C. B. Thompson, ATP citrate lyase is an important component of cell growth and transformation. *Oncogene* **24**, 6314–6322 (2005).
23. K. S. Lucenay, I. Doostan, C. Karakas, T. Bui, Z. Ding, G. B. Mills, K. K. Hunt, K. Keyomarsi, Cyclin E associates with the lipogenic enzyme ATP-citrate lyase to enable malignant growth of breast cancer cells. *Cancer Res.* **76**, 2406–2418 (2016).
24. N. Zaidi, I. Royaux, J. V. Swinnen, K. Smans, ATP citrate lyase knockdown induces growth arrest and apoptosis through different cell- and environment- dependent mechanisms. *Mol. Cancer Ther.* **11**, 1925–1935 (2012).
25. G. Hatzivassiliou, F. Zhao, D. E. Bauer, C. Andreadis, A. N. Shaw, D. Dhanak, S. R. Hingorani, D. A. Tuveson, C. B. Thompson, ATP citrate lyase inhibition can suppress tumor cell growth. *Cancer Cell* **8**, 311–321 (2005).
26. D. Wang, L. Yin, J. Wei, Z. Yang, ATP citrate lyase is increased in human breast cancer, depletion of which promotes apoptosis. *Tumour Biol.* **39**, 1010428317698338 (2017).
27. C. M. Metallo, P. A. Gameiro, E. L. Bell, K. R. Mattaini, J. Yang, K. Hiller, C. M. Jewell, Z. R. Johnson, D. J. Irvine, L. Guarente, J. K. Kelleher, M. G. Vander Heiden, O. Iliopoulos, G. Stephanopoulos, Reductive glutamine metabolism by IDH1 mediates lipogenesis under hypoxia. *Nature* **481**, 380–384 (2012).
28. M. G. Badur, T. Muthusamy, S. J. Parker, S. Ma, S. K. McBrayer, T. Cordes, J. H. Magana, K.-L. Guan, C. M. Metallo, Oncogenic R132 IDH1 mutations limit NADPH for de novo lipogenesis through (D)2-hydroxyglutarate production in fibrosarcoma cells. *Cell Rep.* **25**, 1018–1026.e4 (2018).
29. Z. T. Schug, J. Vande Voorde, E. Gottlieb, The metabolic fate of acetate in cancer. *Nat. Rev. Cancer* **16**, 708–717 (2016).
30. T. Fujino, J. Kondo, M. Ishikawa, K. Morikawa, T. T. Yamamoto, Acetyl-CoA synthetase 2, a mitochondrial matrix enzyme involved in the oxidation of acetate. *J. Biol. Chem.* **276**, 11420–11426 (2001).
31. Z. T. Schug, B. Peck, D. T. Jones, Q. Zhang, S. Grosskurth, I. S. Alam, L. M. Goodwin, E. Smethurst, S. Mason, K. Blyth, L. McGarry, D. James, E. Shanks, G. Kalna, R. E. Saunders, M. Jiang, M. Howell, F. Lassailly, M. Z. Thin, B. Spencer-Dene, G. Stamp, N. J. F. van den Broek, G. Mackay, V. Bulusu, J. J. Kamphorst, S. Tardito, D. Strachan, A. L. Harris, E. O. Aboagye, S. E. Critchlow, M. J. O. Wakelam, A. Schulze, E. Gottlieb, Acetyl-CoA synthetase 2 promotes acetate utilization and maintains cancer cell growth under metabolic stress. *Cancer Cell* **27**, 57–71 (2015).
32. S. A. Comerford, Z. Huang, X. Du, Y. Wang, L. Cai, A. K. Witkiewicz, H. Walters, M. N. Tantawy, A. Fu, H. C. Manning, J. D. Horton, R. E. Hammer, S. L. Mcknight, B. P. Tu, Acetate dependence of tumors. *Cell* **159**, 1591–1602 (2014).
33. T. Mashimo, K. Pichumani, V. Vemireddy, K. J. Hatanpaa, D. K. Singh, S. Sirasanagandla, S. Nannepaga, S. G. Piccirillo, Z. Kovacs, C. Foong, Z. Huang, S. Barnett, B. E. Mickey, R. J. Deberardinis, B. P. Tu, E. A. Maher, R. M. Bachoo, Acetate is a bioenergetic substrate for human glioblastoma and brain metastases. *Cell* **159**, 1603–1614 (2014).
34. J. J. Kamphorst, M. K. Chung, J. Fan, J. D. Rabinowitz, Quantitative analysis of acetyl-CoA production in hypoxic cancer cells reveals substantial contribution from acetate. *Cancer Metab.* **2**, 23 (2014).
35. B. Yenilmez, M. Kelly, G. Zhang, N. Wetoska, O. R. Ilkayeva, K. Min, L. Rowland, C. DiMarzio, W. He, N. Raymond, L. Lifshitz, M. Pan, X. Han, J. Xie, R. H. Friedline, J. K. Kim, G. Gao, M. A. Herman, C. B. Newgard, M. P. Czech, Paradoxical activation of transcription factor SREBP1c and de novo lipogenesis by hepatocyte-selective ATP-citrate lyase depletion in obese mice. *J. Biol. Chem.* **298**, 102401 (2022).
36. S. Zhao, A. M. Torres, R. A. Henry, S. Trefely, M. Wallace, J. V. Lee, A. Carrer, A. Sengupta, S. L. Campbell, Y. M. Kuo, A. J. Frey, N. Meurs, J. M. Viola, I. A. Blair, A. M. Weljie, C. M. Metallo, N. W. Snyder, A. J. Andrews, K. E. Wellen, ATP-citrate lyase controls a glucose-to-acetate metabolic switch. *Cell Rep.* **17**, 1037–1052 (2016).
37. F. Bian, T. Kasumov, K. K. Thomas, K. A. Jobbins, F. David, P. E. Minkler, C. L. Hoppel, H. Brunengraber, Peroxisomal and mitochondrial oxidation of fatty acids in the heart,

assessed from the 13C labeling of malonyl-CoA and the acetyl moiety of citrate. *J. Biol. Chem.* **280**, 9265–9271 (2005).
38. A. E. Reszko, T. Kasumov, F. David, K. A. Jobbins, K. R. Thomas, C. L. Hoppel, H. Brunengraber, C. Des Rosiers, Peroxisomal fatty acid oxidation is a substantial source of the acetyl moiety of malonyl-CoA in rat heart. *J. Biol. Chem.* **279**, 19574–19579 (2004).
39. T. Kasumov, J. E. Adams, F. Bian, F. David, K. R. Thomas, K. A. Jobbins, P. E. Minkler, C. L. Hoppel, H. Brunengraber, Probing peroxisomal β-oxidation and the labelling of acetyl-CoA proxies with [1-^{13}C]octanoate and [3-^{13}C]octanoate in the perfused rat liver. *Biochem. J.* **389**, 397–401 (2005).
40. A. He, X. Chen, M. Tan, Y. Chen, D. Lu, X. Zhang, J. M. Dean, B. Razani, I. J. Lodhi, Acetyl-CoA derived from hepatic peroxisomal β-oxidation inhibits autophagy and promotes steatosis via mTORC1 activation. *Mol. Cell* **79**, 30–42.e4 (2020).
41. S. Zha, S. Ferdinandusse, J. L. Hicks, S. Denis, T. A. Dunn, R. J. Wanders, J. Luo, A. M. De Marzo, W. B. Isaacs, Peroxisomal branched chain fatty acid β-oxidation pathway is upregulated in prostate cancer. *Prostate* **63**, 316–323 (2005).
42. L. Jiang, A. A. Shestov, P. Swain, C. Yang, S. J. Parker, Q. A. Wang, L. S. Terada, N. D. Adams, M. T. Mccabe, B. Pietrak, S. Schmidt, C. M. Metallo, B. P. Dranka, B. Schwartz, R. J. Deberardinis, Reductive carboxylation supports redox homeostasis during anchorage-independent growth. *Nature* **532**, 255–258 (2016).
43. J. Son, C. A. Lyssiotis, H. Ying, X. Wang, S. Hua, M. Ligorio, R. M. Perera, C. R. Ferrone, E. Mullarky, N. Shyh-Chang, Y. Kang, J. B. Fleming, N. Bardeesy, J. M. Asara, M. C. Haigis, R. A. Depinho, L. C. Cantley, A. C. Kimmelman, Glutamine supports pancreatic cancer growth through a KRAS-regulated metabolic pathway. *Nature* **496**, 101–105 (2013).
44. A. Kumar, T. Cordes, A. E. Thalacker-Mercer, A. M. Pajor, A. N. Murphy, C. M. Metallo, NaCT/SLC13A5 facilitates citrate import and metabolism under nutrient-limited conditions. *Cell Rep.* **36**, 109701 (2021).
45. X. Gao, S.-H. Lin, F. Ren, J.-T. Li, J.-J. Chen, C.-B. Yao, H.-B. Yang, S.-X. Jiang, G.-Q. Yan, D. Wang, Y. Wang, Y. Liu, Z. Cai, Y.-Y. Xu, J. Chen, W. Yu, P.-Y. Yang, Q.-Y. Lei, Acetate functions as an epigenetic metabolite to promote lipid synthesis under hypoxia. *Nat. Commun.* **7**, 11960 (2016).
46. W. S. Yang, K. J. Kim, M. M. Gaschler, M. Patel, M. S. Shchepinov, B. R. Stockwell, Peroxidation of polyunsaturated fatty acids by lipoxygenases drives ferroptosis. *Proc. Natl. Acad. Sci. U.S.A.* **113**, E4966–E4975 (2016).
47. O. Feron, The many metabolic sources of acetyl-CoA to support histone acetylation and influence cancer progression. *Ann. Transl. Med.* **7**, S277–S277 (2019).
48. M. Wallace, C. R. Green, L. S. Roberts, Y. M. Lee, J. L. McCarville, J. Sanchez-Gurmaches, N. Meurs, J. M. Gengatharan, J. D. Hover, S. A. Phillips, T. P. Ciaraldi, D. A. Guertin, P. Cabrales, J. S. Ayres, D. K. Nomura, R. Loomba, C. M. Metallo, Enzyme promiscuity drives branched-chain fatty acid synthesis in adipose tissues. *Nat. Chem. Biol.* **14**, 1021–1031 (2018).
49. L. Izzo1, The carnitine shuttle links mitochondrial metabolism to histone acetylation and lipogenesis. *Co-submitted* (2022).
50. X. Liu, D. E. Cooper, A. A. Cluntun, M. O. Warmoes, S. Zhao, M. A. Reid, J. Liu, P. J. Lund, M. Lopes, B. A. Garcia, K. E. Wellen, D. G. Kirsch, J. W. Locasale, Acetate production from glucose and coupling to mitochondrial metabolism in mammals. *Cell* **175**, 502–513.e13 (2018).
51. I. J. Lodhi, C. F. Semenkovich, Peroxisomes: A nexus for lipid metabolism and cellular signaling. *Cell Metab.* **19**, 380–392 (2014).
52. O. Apanasets, C. P. Grou, P. P. Van Veldhoven, C. Brees, B. Wang, M. Nordgren, G. Dodt, J. E. Azevedo, M. Fransen, PEX5, the shuttling import receptor for peroxisomal matrix proteins, is a redox-sensitive protein. *Traffic* **15**, 94–103 (2014).
53. C. Van den Branden, F. Roels, Thioridazine: A selective inhibitor of peroxisomal β-oxidation in vivo. *FEBS Lett.* **187**, 331–333 (1985).
54. R. Shi, Y. Zhang, Y. Shi, S. Shi, L. Jiang, Inhibition of peroxisomal β-oxidation by thioridazine increases the amount of VLCFAs and Aβ generation in the rat brain. *Neurosci. Lett.* **528**, 6–10 (2012).
55. R. J. A. Wanders, H. R. Waterham, S. Ferdinandusse, Metabolic interplay between peroxisomes and other subcellular organelles including mitochondria and the endoplasmic reticulum. *Front. Cell Dev. Biol.* **3**, 83 (2016).
56. B. S. Jakobs, R. J. A. Wanders, Fatty acid $β$-oxidation in peroxisomes and mitochondria: The first, unequivocal evidence for the involvement of carnitine in shuttling propionyl-CoA from peroxisomes to mitochondria. *Biochem. Biophys. Res. Commun.* **213**, 1035–1041 (1995).
57. F. Leighton, S. Bergseth, T. Rortveit, E. N. Christiansen, J. Bremer, Free acetate production by rat hepatocytes during peroxisomal fatty acid and dicarboxylic acid oxidation. *J. Biol. Chem.* **264**, 10347–10350 (1989).
58. J. Hsu, N. Fatuzzo, N. Weng, W. Michno, W. Dong, M. Kienle, Y. Dai, A. Pasca, M. Abu-Remaileh, N. Rasgon, B. Bigio, C. Nasca, C. Khosla, Carnitine octanoyltransferase is important for the assimilation of exogenous acetyl-L-carnitine into acetyl-CoA in mammalian cells. *J. Biol. Chem.* **299**, 102848 (2022).
59. Y.-I. Kim, I.-K. Nam, D.-K. Lee, S. Bhandari, L. Charton, S. A. Kwak, J.-Y. Lim, K. H. Hong, S.-J. Kim, J. N. Lee, S. W. Kwon, H.-S. So, N. Linka, R. Park, S.-K. Choe, Slc25a17 acts as a peroxisomal coenzyme A transporter and regulates multiorgan development in zebrafish. *J. Cell. Physiol.* **235**, 151–165 (2020).
60. A. Baker, D. J. Carrier, T. Schaedler, H. R. Waterham, C. W. Van Roermund, F. L. Theodoulou, Peroxisomal ABC transporters: Functions and mechanism. *Biochem. Soc. Trans.* **43**, 959–965 (2015).
61. A. Carrer, S. Trefely, S. Zhao, S. L. Campbell, R. J. Norgard, K. C. Schultz, S. Sidoli, J. L. D. Parris, H. C. Affronti, S. Sivanand, S. Egolf, Y. Sela, M. Trizzino, A. Gardini, B. A. Garcia, N. W. Snyder, B. Z. Stanger, K. E. Wellen, Acetyl-CoA metabolism supports multistep pancreatic tumorigenesis. *Cancer Discov.* **9**, 416–435 (2019).
62. J. M. Bae, J. H. Kim, H. J. Oh, H. E. Park, T. H. Lee, N. Cho, G. H. Kang, Downregulation of acetyl-CoA synthetase 2 is a metabolic hallmark of tumor progression and aggressiveness in colorectal carcinoma. *Mod. Pathol.* **30**, 267–277 (2016).
63. V. Bulusu, S. Tumanov, E. Michalopoulou, N. J. Van Den Broek, G. Mackay, C. Nixon, S. Dhayade, Z. T. Schug, J. Vande Voorde, K. Blyth, E. Gottlieb, A. Vazquez, J. J. Kamphorst, Acetate recapturing by nuclear acetyl-CoA synthetase 2 prevents loss of histone acetylation during oxygen and serum limitation. *Cell Rep.* **18**, 647–658 (2017).
64. L. Yao, L. Jiang, F. Zhang, M. Li, B. Yang, F. Zhang, X. Guo, Acetate promotes SNAI1 expression by ACSS2-mediated histone acetylation under glucose limitation in renal cell carcinoma cell. *Biosci. Rep.* **40**, BSR20200382 (2020).
65. S. Trefely, C. D. Lovell, N. W. Snyder, K. E. Wellen, Compartmentalised acyl-CoA metabolism and roles in chromatin regulation. *Mol. Metab.* **38**, 100941 (2020).
66. A. Luengo, D. Y. Gui, M. G. Vander Heiden, Targeting metabolism for cancer therapy. *Cell Chem. Biol.* **24**, 1161–1180 (2017).
67. C. W. van Roermund, E. H. Hettema, M. van den Berg, H. F. Tabak, R. J. Wanders, Molecular characterization of carnitine-dependent transport of acetyl-CoA from peroxisomes to mitochondria in Saccharomyces cerevisiae and identification of a plasma membrane carnitine transporter, Agp2p. *EMBO J.* **18**, 5843–5852 (1999).
68. S. M. Houten, R. J. A. Wanders, P. Ranea-Robles, Metabolic interactions between peroxisomes and mitochondria with a special focus on acylcarnitine metabolism. *Biochim. Biophys. Acta Mol. Basis Dis.* **1866**, 165720 (2020).
69. J. D. Young, INCA: A computational platform for isotopically non-stationary metabolic flux analysis. *Bioinformatics* **30**, 1333–1335 (2014).
70. T. Cordes, C. M. Metallo, Quantifying intermediary metabolism and lipogenesis in cultured mammalian cells using stable isotope tracing and mass spectrometry, in *High-Throughput Metabolomics: Methods and Protocols*, A. D'Alessandro, Ed. (Springer New York, 2019), pp. 219–241; https://doi.org/10.1007/978-1-4939-9236-2_14.
71. F. A. Ran, P. D. Hsu, J. Wright, V. Agarwala, D. A. Scott, F. Zhang, Genome engineering using the CRISPR-Cas9 system. *Nat. Protoc.* **8**, 2281–2308 (2013).
72. N. E. Sanjana, O. Shalem, F. Zhang, Improved vectors and genome-wide libraries for CRISPR screening. *Nat. Methods* **11**, 783–784 (2014).
73. S. Kim, D. Kim, S. W. Cho, J. Kim, J. S. Kim, Highly efficient RNA-guided genome editing in human cells via delivery of purified Cas9 ribonucleoproteins. *Genome Res.* **24**, 1012–1019 (2014).
74. A. Kumar, J. Mitchener, Z. A. King, C. M. Metallo, Escher-Trace: A web application for pathway-based visualization of stable isotope tracing data. *BMC Bioinformatics* **21**, 297 (2020).

Acknowledgments: We thank all members of the Metallo laboratory for support and helpful discussions. We thank S. Zhao for helping with generating PEX5KO cell lines. ACLY and ACSS2 cellular reagents were provided by Nimbus Therapeutics. Figure panels were made with BioRender. **Funding:** This work was supported by U.S. National Institutes of Health (NIH) grants R35CA220538 and P01CA120964 (to R.J.S.) and R01CA234245 (to C.M.M.). A.K. was supported in part by U54CA132379, and H.G. was supported in part by T32DK007541. ACLY-, ACSS2-, and ACLY/ACSS2 DKO-A549 cell lines were provided as in-kind support from Nimbus Discovery. **Author contributions:** R.S.K., A.K., R.U.S., and C.M.M. conceived and designed the study. R.S.K. and A.K. performed experiments. R.S.K. generated the *PEX5*-KO cell lines. H.G. and R.J.S. provided 643T cell lines and advised on studies. R.S.K., G.H.M., and C.R.G. performed LC-MS/MS lipidomic analytics. T.C. performed the ferroptosis assay. R.S.K., A.K., and C.M.M wrote the paper with input from all authors. **Competing interests:** R.J.S. is an employee of Nimbus Therapeutics and holds private equity in the company. The authors declare that they have no other competing interests. **Data and materials availability:** All data needed to evaluate the conclusions in the paper are present in the paper and/or the Supplementary Materials. Please contact Nimbus Discovery to obtain ACLY-, ACSS2-, and ACLY/ACSS2 DKO-A549 cell lines.

Submitted 23 September 2022
Accepted 3 April 2023
Published 3 May 2023
10.1126/sciadv.adf0138